# LRRK2 activation in idiopathic Parkinson's disease

Di Maio, Roberto; Hoffman, Eric K.; Rocha, Emily M.; Keeney, Matthew T.; Sanders, Laurie H.; De Miranda, Briana R.

*Published in:*
Science Translational Medicine

*DOI:*
10.1126/scitranslmed.aar5429

*Publication date:*
2018

*Document Version*
Peer reviewed version

# A Central Role for LRRK2 in Idiopathic Parkinson Disease

**Summary:** *Wildtype LRRK2 is activated in dopamine neurons in idiopathic Parkinson disease and plays a pathogenic role in the disease.*

Roberto Di Maio[1,2,3], Eric K. Hoffman[1,2], Emily M. Rocha[1,2], Matthew T. Keeney[1,2], Laurie H. Sanders[1,2,4], Briana R. De Miranda[1,2], Alevtina Zharikov[1,2], Amber Van Laar[1,2], Antonia Stepan[5], Thomas A. Lanz[5], Julia K. Kofler[6], Edward A. Burton[1,2,7], Dario R. Alessi[8], Teresa G. Hastings[1,2], J. Timothy Greenamyre[1,2,7,†]

[†]Correspondence should be addressed to JTG (jgreena@pitt.edu).

[1]Pittsburgh Institute for Neurodegenerative Diseases, University of Pittsburgh, Pittsburgh, Pennsylvania. [2]Department of Neurology, University of Pittsburgh, Pittsburgh, Pennsylvania. [3]Ri.MED Foundation, Palermo, Italy. [4]Department of Neurology, Duke University, Durham, North Carolina. [5]Worldwide Medicinal Chemistry, Pfizer Worldwide Research and Development, Cambridge, Massachusetts. [6]Department of Pathology, University of Pittsburgh, Pittsburgh, Pennsylvania. [7]Geriatric Research, Education and Clinical Center, VA Pittsburgh Healthcare System, Pittsburgh, Pennsylvania. [8]MRC Protein Phosphorylation and Ubiquitylation Units, University of Dundee, Dundee, Scotland.

**Correspondence:**

J. Timothy Greenamyre
University of Pittsburgh
3501 Fifth Avenue, Suite 7039
Pittsburgh, PA 15260

Tel: 412-648-9793
Fax: 412-648-9766
Email: jgreena@pitt.edu

**SUMMARY**

Abnormally increased kinase activity due to mutations in the leucine rich repeat kinase 2 (LRRK2) gene is the cause of Parkinson disease (PD) in about 3-4% of people with the disease. We now show that, in the brains of individuals with idiopathic PD, LRRK2 kinase activity is aberrantly increased in vulnerable dopamine neurons by oxidative mechanisms involving α-synuclein and mitochondrial impairment – and this causes endolysosomal dysfunction and accumulation of phosphorylated α-synuclein. Thus, independent of mutation, activation of LRRK2 kinase activity contributes importantly to pathogenesis, suggesting inhibition of LRRK2 kinase activity will be useful for the majority of PD patients.

**ABSTRACT**

Missense mutations in leucine-rich repeat kinase 2 (LRRK2) cause familial Parkinson disease (PD); however, the role of wildtype LRRK2 in idiopathic PD (iPD) is unclear. Here, we show that wildtype LRRK2 kinase activity is selectively enhanced in substantia nigra dopamine neurons in idiopathic PD and two different animal models of the disease. This occurs through ROS signaling, resulting in phosphorylation of the LRRK2 substrate Rab10 and other downstream consequences including abnormalities of mitochondrial protein import and lysosomal function. Overall, our work shows that, independent of mutations, wildtype LRRK2 plays a key role in idiopathic PD. LRRK2-directed therapeutics may therefore be useful for most people with PD.

**INTRODUCTION**

Parkinson's disease (PD) is a common neurodegenerative disease that results in motor impairment, cognitive and psychiatric symptoms and autonomic dysfunction (*1*). While numerous gene mutations are known to cause familial PD, about 90% of cases are "idiopathic" (iPD). LRRK2 missense mutations are the most common cause of autosomal dominant PD, and may account for about 3% of cases overall (*2, 3*). The *LRRK2* locus also contains a risk factor for iPD (*4*), but the role of LRRK2 in typical iPD is unknown. It is generally believed that the common missense mutations in LRRK2 confer a toxic gain-of-function and increased LRRK2 kinase activity has been strongly implicated in pathogenesis (*5*). Among the kinase substrates of LRRK2 are a subset of the Rab GTPases, including Rab10, which has been implicated in maintenance of endoplasmic reticulum, vesicle trafficking and autophagy (*6*). LRRK2-induced phosphorylation of Rab10 inhibits its function by preventing binding to Rab GDP-dissociation inhibitor factors necessary for membrane delivery and recycling. As such, aberrantly enhanced LRRK2 kinase activity is likely associated with reduced activity of Rab10 and its effectors.

Assessment of the kinase activity state of LRRK2 under various conditions has been somewhat cumbersome, although there appears to be a growing consensus that autophosphorylation at Ser1292 correlates with activity (*7, 8*). Phosphoserine1292 (pS1292) has generally been detected by western blotting rather than immunocytochemistry, which limits anatomical or cellular resolution. LRRK2 is believed to be a rather low-abundance protein, and efforts to detect it immunocytochemically sometimes rely on high antibody concentrations, which may reduce specificity. This problem may be compounded for pS1292 when only a fraction of the total (small) pool of LRRK2 is phosphorylated. The activity of LRRK2 is also regulated by its interaction with 14-3-3 proteins, whose binding to LRRK2 requires phosphorylation at LRRK2 serine residues 910 and 935 (*9, 10*), which are not autophosphorylation sites. Although the binding of LRRK2 to 14-3-3 protein is associated with reduced kinase activity (*11*), this interaction can be disrupted by oxidative stressors, including $H_2O_2$ (*12*). The

interaction between LRRK2 and 14-3-3 has generally been assessed by co-immunoprecipitation. A critical barrier to understanding the role of LRRK2 in iPD has been the absence of a practical, sensitive, high-resolution assay for its activation state.

We have developed and validated novel proximity ligation (PL) assays with excellent anatomical resolution that can rapidly provide information regarding activation state, cellular localization and physiological regulators of LRRK2. The assay is based on (i) S1292 phosphorylation and (ii) dissociation of 14-3-3 from LRRK2. Using this and other assays, we provide evidence that LRRK2 is activated oxidatively by mitochondrial impairment or α-synuclein overexpression and that it plays a central role in iPD pathogenesis by regulating autophagy and pSer129-α-synuclein levels.

## RESULTS

### Assay development and validation

As a LRRK2 autophosphorylation site, pSer1292 reflects the activity of LRRK2 *per se*. As such, we developed a proximity ligation assay to amplify the signal and increase the specificity of an antibody recognizing the pSer1292 epitope of the protein. For the PL assay, we paired the anti-pSer1292 antibody with a validated antibody directed against an epitope in the COR domain of the protein. In this way, the signal of the anti-pSer1292 antibody was amplified and detected only if it was in proximity to the anti-COR domain antibody (i.e., specific LRRK2 pSer1292 signals were amplified, whereas potential signals from non-specific or off-target antibody binding were filtered out by the PL assay). A second PL assay assessed the interaction between LRRK2 and 14-3-3, whose binding to LRRK2 is associated with reduced activity. Thus, the PL assays were designed such that LRRK2 activity should be associated with a strong pSer1292 signal and a weak 14-3-3 signal; conversely, when LRRK2 is inactive there should be little pSer1292 signal and a robust 14-3-3 signal.

To validate the assays, we used wildtype (WT), LRRK2$^{G2019S/G2019S}$ and LRRK2$^{-/-}$ human embryonic kidney- (HEK-) 293 cells, obtained by CRISPR/Cas9 gene editing. In WT cells, there was little pSer1292 signal and a strong 14-3-3 PL signal (**figure 1A, B, D, E**). The G2019S mutation is known to cause increased LRRK2 kinase activity (*5, 6*). Accordingly, in LRRK2$^{G2019S/G2019S}$ cells, there was a bright pSer1292 signal and loss of the 14-3-3 interaction. No signal in either PLA was seen in cells lacking LRRK2 (**figure 1A, B, D, E**), further establishing the specificity of the assays. The small GTPase, Rab10, has recently been shown to be directly phosphorylated at Thr73 by LRRK2 (*6*). Using a specific pThr73-Rab10 antibody, we found low levels of phosphorylated Rab10 in WT cells, and much higher levels in LRRK2$^{G2019S/G2019S}$ cells, in keeping with increased kinase activity of the mutant protein **(figure 1A, C, D)**. After assay development, validation included blinded analysis and correct identification of all 3 cell lines with these assays alone. Using the selective LRRK2 kinase inhibitors, GNE-7915 and MLi-2 (*13*), in

dose-response studies, we found that LRRK2 activation state, assessed by pSer1292 PL signal, correlated closely with phosphorylation of its substrate, Rab10 **(figure 1F, G)**. We next looked at LRRK2 activation state in patient-derived lymphoblastoid cell lines. Relative to cells derived from a healthy age-matched control, in a LRRK2 G2019S mutation carrier, there was marked elevation of the pSer1292 signal and titration with the selective LRRK2 kinase inhibitor, GNE-7915, dose-dependently reduced the pSer1292 PL and pThr73-Rab10 signals in parallel **(figure 1H)**.

To summarize, basal kinase activity of endogenous WT LRRK2, assessed by pSer1292 PL and pThr-Rab10 immunoreactivity was low. This was associated with a strong 14-3-3 PL signal, suggesting a significant interaction with 14-3-3 protein. In cells harboring the pathogenic G2019S mutation, LRRK2 was highly activated (strong pSer1292 PL signal and elevated levels of Rab10 phosphorylation) and there was loss of the 14-3-3 interaction. LRRK2 activation as evaluated by pSer1292 PL and pThr-Rab10 immunoreactivity, was reversed by the LRRK2 kinase inhibitors, GNE-7915 and MLi-2, at appropriate concentrations.

**Endogenous, wildtype LRRK2 is activated in idiopathic PD**

Conventional assays of LRRK2 activity often rely on overexpression, and they require substantial amounts of tissue, lack cellular/anatomical resolution, and cannot be performed in previously fixed tissue. In contrast, our assays can assess the activation state of endogenous LRRK2 on a cell-by-cell basis using fixed cells or tissue. In this context, we measured pSer1292 PL and pThr73-Rab10 by quantitative confocal immunofluorescence in sections of substantia nigra from 7 individuals dying with iPD and from 8 controls matched for age and postmortem interval. In nigrostriatal dopamine neurons from healthy controls, there were very low basal levels of pSer1292 PL and pThr73-Rab10 immunoreactivity signal and a strong 14-3-3 PL signal (**figure 2**). In contrast, the remaining dopamine neurons from the iPD cases showed about a 6-fold increase in pSer1292 PL ($p<0.0002$, two-tailed,

unpaired t-test; $p<0.002$ with Welch's correction for unequal variances), and this was associated with a 4-fold increase in phosphorylation (pThr73) of the LRRK2 substrate Rab10 ($p<0.0002$). The increase in LRRK2 activation state in iPD dopamine neurons corresponded to a 5-fold decrease in the 14-3-3 PL signal ($p<0.0001$; $p<0.0004$ with Welch's correction). Thus, there is evidence that endogenous WT LRRK2 is activated in dopamine neurons in iPD, and this is associated with increased substrate phosphorylation.

In addition to neuronal expression, LRRK2 has also been associated with microglia (*14*). We found detectable levels of pS1292 PL signal in nigral microglia in controls **(figure S1A, B)**, and the signal was more than doubled in microglia from iPD cases ($p<0.0005$, two-tailed, unpaired t-test).

**WT LRRK2 activation is reproduced in mitochondrial and α-synuclein models of PD**

Mitochondrial impairment and α-synuclein accumulation/aggregation have been strongly implicated in PD pathogenesis (*15*). Therefore, we tested whether LRRK2 is similarly activated in rat models based on these mechanisms. First, we used the rotenone model of PD, which has been shown to reproduce or even predict pathological and/or pathogenic features of the disease (*16*). Using substantia nigra sections from rotenone-treated rats that had reached behavioral endpoint (severe parkinsonism after 10-14 days), we found a 10-fold increase in pSer1292 PL signal in nigrostriatal dopamine neurons compared to vehicle-treated controls ($p<0.0001$, unpaired, 2-tail t-test) **(figure 3A-C)**. In these animals, there was a dramatic loss of the 14-3-3 PL signal ($p<0.0001$, unpaired, 2-tail t-test) similar to the changes we observed in human brain. As in iPD brains, we found detectable pS1292 PL signal in control microglia **(figure S1C,D)**, and the signal was more than doubled after rotenone treatment ($p<0.05$, unpaired, 2-tail t-test). To determine whether LRRK2 activation occurs prior to neurodegeneration, we examined tissue from animals that received only 1 or 5 days of rotenone, time points at which we detect no degeneration of the nigrostriatal neurons **(figure S2)**. After a single dose of rotenone,

pSer1292 PL signal was increased 5-fold relative to vehicle treatment ($p<0.0001$, ANOVA with Bonferroni correction), and after 5 daily doses, the PL signal was increased 6-fold ($p<0.0001$). These results indicate that mitochondrial impairment can lead to activation of LRRK2 well before there is any neurodegeneration.

α-Synuclein accumulation and Lewy pathology are hallmarks of PD. Elevated levels of WT α-synuclein may cause PD, and several groups have used viral vector-mediated overexpression of α-synuclein as a model of PD (*17*). Here, we used adeno-associated virus type 2 (AAV2)-mediated overexpression of wildtype human α-synuclein (*hSNCA*) injected unilaterally into substantia nigra pars compacta to induce slowly progressive neurodegeneration. Six weeks after vector injection, when degeneration is ongoing, remaining nigrostriatal neurons showed a marked 10-fold increase in pSer1292 PL signal compared to the contralateral, uninjected hemisphere ($p<0.0001$, paired 2-tail t-test) – and there was a concomitant loss of the 14-3-3 PL signal ($p<0.0001$) **(figure 3D-F)**.

Both rotenone treatment and AAV2-mediated α-synuclein overexpression lead to oligomerization of α-synuclein, as well as accumulation of Ser129-phosphorylated α-synuclein (*18, 19*). We recently identified soluble oligomers and pSer129-α-synuclein as specific forms of α-synuclein that have deleterious effects on mitochondrial protein import machinery and which cause mitochondrial impairment (*15*). In analogous fashion, when *SNCA*$^{-/-}$ cells were treated with exogenous soluble oligomers of α-synuclein (400 nM monomer equivalent) for 24 hours, there was marked activation of endogenous WT LRRK2 with increased pSer1292 and loss of 14-3-3 PL signals **(figure S3)** ($p<0.0001$, ANOVA with Bonferroni correction). Treatment with monomeric α-synuclein did not activate LRRK2.

Both rotenone treatment and elevated α-synuclein increase formation of reactive oxygen species (ROS) and both insults activate WT LRRK2, which raises the possibility that it is secondary generation of ROS

that actually activates LRRK2. To test directly whether ROS can activate LRRK2, we treated WT cells with $H_2O_2$ **(figure 4A, B)**. Treatment with $H_2O_2$ dose-dependently (50 nM – 5 μM) activated the pSer1292 PL signal ($p<0.0001$ vs. control for all $H_2O_2$ doses; 1-way ANOVA with Bonferroni correction) and increased phosphorylation of its substrate, Rab10 ($p<0.0001$ for all doses above 50 nM $H_2O_2$). The antioxidant, α-tocopherol, blocked $H_2O_2$ activation of the pSer1292 signal ($p<0.0001$) and Rab10 phosphorylation ($p<0.0001$).

Further evidence of oxidative activation of LRRK2 resulted from study of endogenous NADPH oxidase 2 (NOX2). As *in vivo*, we found that rotenone treatment of WT HEK-293 cells caused an increased pSer1292 PL signal and Rab10 phosphorylation **(figure 4C-E)**. Although rotenone may cause mitochondrial ROS formation, mitochondrially-derived ROS may also activate NOX2 in a process known as ROS-induced ROS release, which can feed forward to amplify ROS production (*20, 21*). We found that co-treatment with rotenone plus the specific NOX2 inhibitor peptide, Nox2ds-tat (*22*), blocked rotenone's effects on LRRK2 activation and phosphorylation of its substrate ($p<0.0001$, 1-way ANOVA with Bonferroni correction). Thus, NOX2-generated superoxide appears to be important in activating LRRK2.

***In vivo* treatment with a LRRK2 kinase inhibitor blocks rotenone-induced activation of nigrostriatal LRRK2 and has beneficial effects on pSer129-α-synuclein levels and markers of autophagy & lysosomes.**

The rotenone model of PD reproduces many features of the human disease, including accumulation of pSer129-α-synuclein, impairment of autophagy, reduced mitochondrial protein import (*15*), and now, activation of endogenous WT LRRK2 in nigrostriatal dopamine neurons. To determine whether systemic treatment with a brain-penetrant LRRK2 inhibitor could block rotenone-induced LRRK2 activation, and to survey some of the potential downstream effects of LRRK2 activation, rats were

treated for 5 days with rotenone (2.8 mg/kg/day, i.p.) with or without concomitant PF-360 (10 mg/kg p.o. twice daily), a highly selective LRRK2 kinase inhibitor (*23, 24*). This PF-360 dosing regimen results in a pharmacokinetic profile in which an $IC_{90}$ concentration in brain is achieved for 15 hours daily and an $IC_{50}$ concentration is achieved for a full 24 hours.

In a new cohort of rats treated with rotenone for 5 days, there was a marked increase in pSer1292 PL signal in nigrostriatal neurons, which was associated with an increase in phosphorylation of Rab10 (**figure 5A-C**). Co-treatment with PF-360 effectively blocked the rotenone-induced activation of LRRK2 ($p<0.0001$, two-way ANOVA, Sidak's correction) and phosphorylation of Rab10 ($p<0.0001$). Thus, the pSer1292 PL assay provided an *ex vivo* assay of target (LRRK2) engagement by PF-360, which was corroborated by measurement of pThr73-Rab10.

We reported previously that chronic rotenone treatment (10-14 days) leads to elevated levels of pSer129-α-synuclein (*15*). Here we found that the rats treated for only 5 days also accumulated pSer129-α-synuclein, and co-treatment with PF-360 prevented this accumulation **(figure 5D, E)**. The mechanism by which pSer129-α-synuclein accrues in response to rotenone is uncertain, but it has been suggested that phosphorylation of α-synuclein at ser129 targets the protein for degradation by autophagy (*25, 26*). Both chaperone-mediated autophagy (CMA) and macroautophagy play roles in α-synuclein degradation (*27, 28*). Therefore, we assessed a marker for CMA, Lamp2A, which is located on lysosomes, and another marker, Lamp1, which may label late endosomes, autolysosomes or lysosomes. There were abundant Lamp2A and Lamp1 punctae in dopamine neurons from vehicle treated rats, which were dramatically lost after rotenone treatment, and preserved by co-treatment with PF-360 **(figure 6A-E)**. Together, these results indicate that there is early profound impairment of CMA and lysosomal function which is downstream of LRRK2 kinase activity. Additionally, these results suggest that pSer129-α-synuclein accumulates in rotenone treated rats because of LRRK2-induced CMA and

lysosomal dysfunction – and LRRK2 kinase inhibition prevents this. To complement these pharmacological studies, we examined the effects of rotenone on pSer129-α-synuclein in WT and LRRK2$^{-/-}$ HEK cells. As *in vivo*, we found that rotenone treatment caused accumulation of pSer129-α-synuclein in WT cells; however, there was no such accumulation in the LRRK2 null cells (**Figure S4**), thereby providing further evidence that buildup of pSer129-α-synuclein is LRRK2-dependent. Moreover, the rotenone-induced increase in pSer129-α-synuclein in WT cells was effectively blocked by PF-360 to the same extent as in LRRK2$^{-/-}$ cells, confirming the specificity of the PF-360 effect.

Similar to rotenone-treated rats, there was a dramatic loss of Lamp1 puncta in human brain specimens from individuals with iPD ($p<0.001$, unpaired 2-tail t-test) and this was accompanied by an accumulation of the autophagy cargo receptor, p62/SQSTM1 ($p<0.03$), into Lewy bodies, indicating autophagic and lysosomal dysfunction **(figure 6F, G)**. As reported by many other groups, and as seen in rotenone-treated rats, there is accumulation of pSer129-α-synuclein in substantia nigra in iPD.

*In vitro* experiments have shown that pSer129-α-synuclein binds to TOM20 and inhibits mitochondrial protein import; however, this has not been examined directly in human brain or in the rotenone rat. Examination of human iPD brains **(figure 7A,B)** revealed a marked increase of pSer129-α-synuclein-TOM20 PL signal ($p<0.0001$, unpaired, 2-tail t-test), indicating that accumulation of this specific form of α-synuclein has toxic consequences in terms of mitochondrial protein import. Similarly, in the rotenone rats **(figure 7C-E)**, the increased pSer129-α-synuclein we found at 5 days was associated with its binding to TOM20, measured as a strong pSer129-α-synuclein-TOM20 PL signal ($p<0.0001$, 2-way ANOVA with Bonferroni correction), as well as reduced levels and redistribution of the imported complex I subunit, Ndufs3, from mitochondria to cytosol ($P<0.0001$). Co-treatment with PF-360 prevented the elevation in pSer129-α-synuclein levels **(figure 5E)** and, as a result, there was little binding to TOM20 ($p<0.0001$ vs rotenone alone), and there was preservation of normal levels and

mitochondrial localization of Ndufs3 **(figure 7C,E)**. Thus, both the accumulation of pSer129-α-synuclein and its toxic consequences appear to be downstream of LRRK2 kinase activity.

**DISCUSSION**

Development of a new assay allowed us to show that endogenous WT LRRK2 is activated in nigrostriatal dopamine neurons in iPD – and this can be reproduced in rodent models of the disease. While our new assay does not measure activity *per se*, it provides a snapshot of relative LRRK2 activation state and does so with a cellular level of resolution (e.g., in dopamine neurons and microglia). The assay was validated (i) by using gene-edited cells, (ii) by demonstrating that the readout of LRRK2 activation state (pSer1292 PL signal) correlates with substrate (Rab10) phosphorylation levels, and (iii) by showing that both the pSer1292 PL and pThr73-Rab10 signals respond appropriately and in parallel to 3 structurally distinct LRRK2 kinase inhibitors (GNE-7915, MLi-2 and PF-360). Consistent with our results, others showed recently, by means of immunoblotting, that the phosphorylation state of LRRK2 (at Ser935) correlates with Rab10 phosphorylation in dose-response studies using PF-360 (*23*).

The finding that treatment of G2019S mutant engineered or patient-derived cells with kinase inhibitors blocks the pSer1292 PL signal indicates that this readout is readily reversible. Thus, the relative degree of LRRK2 activation detected reflects the physiological state of LRRK2 in the cell or tissue at the specific time of fixation. Additionally, the ease with which inhibitor dose-response relationships can be assessed suggests the assay can provide a quantitative measure of target (LRRK2) engagement.

Recent work from West and colleagues showed that genetic ablation or pharmacological kinase inhibition of endogenous WT LRRK2 reduced the toxicity of AAV2-*hSNCA* injected into substantia nigra, suggesting a possible role of LRRK2 in α-synuclein toxicity (*29, 30*). Implicit in such a conclusion is the assumption that WT LRRK2 kinase must be active in nigrostriatal neurons under these experimental conditions; however, this has been difficult to demonstrate with conventional assays. Consistent with this supposition, we found that AAV2-*hSNCA* (as used by West and colleagues) activates LRRK2 in

nigrostriatal neurons. In this context, our findings indicate that LRRK2 is activated in the vulnerable dopamine neurons in human iPD and suggest that endogenous WT LRRK2 may play a role pathogenesis.

Our assay allows relatively facile assessment of physiological regulators of LRRK2 activity. In cell culture, we showed that low concentrations of oligomeric, but not monomeric, α-synuclein activate LRRK2. We recently reported that oligomeric, but not monomeric, α-synuclein binds to TOM20, impairs mitochondrial protein import, and causes mitochondrial dysfunction and aberrant ROS production (*15*). Similarly, the mitochondrial toxin rotenone induces ROS production, and we showed that it caused LRRK2 activation and LRRK2 substrate phosphorylation. Interestingly, the rotenone-induced activation of LRRK2 was blocked by inhibition of NOX2, implicating ROS-induced ROS release and NOX2-derived superoxide in the phenomenon (*20*). To directly test whether ROS can activate LRRK2, cells were treated with physiological concentrations of $H_2O_2$, and this resulted in increased pSer1292 PL signal and concomitant Rab10 phosphorylation. These results suggest that oxidative stress, long implicated in PD pathogenesis, may up-regulate LRRK2 activity. Further, our results are consistent with the work of Mamais et al., which showed that $H_2O_2$ dissociates LRRK2 from 14-3-3 (*12*), and the study by Li et al., which found a small activation of LRRK2 by $H_2O_2$ (*31*). The molecular mechanisms by which ROS stimulate LRRK2 kinase activity are unknown; whether this activation results from direct effects on the LRRK2 protein or from effects on interacting proteins, such as protein phosphatases, remains to be explored.

The consistent finding that LRRK2 is activated in vulnerable dopaminergic neurons in human iPD raises the possibility that LRRK2 kinase activity may play a central role in pathogenesis of most PD cases. To investigate experimentally the possibility that LRRK2 activation may have downstream deleterious effects on putative pathogenic mechanisms, we treated rats for 5 days with rotenone – with or without co-treatment with the LRRK2 kinase inhibitor, PF-360. We found that rotenone (i) activated LRRK2 in

nigrostriatal dopamine neurons; (ii) increased phosphorylation of a LRRK2 substrate, Rab10; (iii) increased levels pSer129-α-synuclein and binding to TOM20; and (iv) disrupted markers of autophagy. All these effects were blocked by PF-360, and we therefore conclude that these mechanisms are downstream of LRRK2 activity (**figure 8**).

Rab10 is a *bona fide* direct substrate of LRRK2 and has been implicated in maintenance of endoplasmic reticulum, vesicle trafficking and autophagy (*32-34*). LRRK2-induced phosphorylation of Rab10 inhibits its function by preventing binding to Rab GDP-dissociation inhibitor factors necessary for membrane delivery and recycling (*6*). Thus, LRRK2 activation leads to Rab10 phosphorylation (and inhibition) and this likely impairs autophagic and/or lysosomal function. Phospho-Rab10-induced autophagic dysfunction, in turn, may account for the early accumulation of pSer129-α-synuclein, which is normally degraded by CMA and macroautophagy. Consistent with our findings, Volpicelli and colleagues reported that the G2019S mutation was associated with accumulation of pSer129-α-synuclein-positive inclusions, which were prevented by LRRK2 kinase inhibitors, including MLi-2 (*35*). It is also noteworthy that pSer129-α-synuclein is one of the species of α-synuclein we reported that binds to TOM20 and impairs mitochondrial function (*15*). The fact that all these abnormalities are prevented by treatment with a LRRK2 kinase inhibitor strongly supports this hypothetical scheme (**figure 8**). Further, our experimental paradigm of surveying potential pathogenic mechanisms in a PD model, with and without concomitant treatment with a LRRK2 kinase inhibitor, will likely lead to new insights into how aberrant LRRK2 activity causes neurodegeneration.

Our study is not without limitations. As noted, the PL assays we employed do not measure activity *per se*; however, several convergent lines of evidence confirm that we measured reliable surrogates of LRRK2 activity: the pS1292 PL signal correlated with substrate (Rab10) phosphorylation and with loss of 14-3-3 binding signal – and both the 1292 PL signal and the pThr72-Rab10 signal were inhibited dose-

dependently by selective LRRK2 kinase inhibitors of different chemical classes. In this context, we provided compelling evidence that wildtype LRRK2 is activated in nigrostriatal neurons in iPD and in rat models thereof. Nevertheless, while LRRK2 activation occurred very early in the course of rotenone-induced parkinsonism, and early intervention with a LRRK2 kinase inhibitor was beneficial, the time course of LRRK2 activation in the human brain is unknown and the clinical effects of LRRK2 inhibitors remain to be examined.

The fact that there are a variety of selective LRRK2 kinase inhibitors reflects the interest by the pharmaceutical industry in target-specific therapeutics for PD, even for the relatively small number of cases caused by LRRK2 mutations. The results presented here provide compelling evidence that WT LRRK2 is activated by PD-relevant relevant stimuli in dopamine neurons in iPD and that this, in turn, triggers a downstream pathological cascade of events culminating in neurodegeneration. As such, rather than being applicable for 3-4% of people with PD, LRRK2-targeted therapeutics may be useful for most, if not all, people with PD.

**MATERIALS AND METHODS**

*Study Design*. This study was designed to assess the role of wildtype LRRK2 in iPD. To do so, we developed new PL assays to assess the phosphorylation state of the LRRK2 autophosphorylation site, Ser1292, and separately, the binding of LRRK2 to 14-3-3, which is associated with decreased LRRK2 kinase activity. These assays were validated using CRISPR/Cas9 genome-edited HEK293 cells and 3 chemically distinct LRRK2 kinase inhibitors. The validated assays were then used to assess LRRK2 activation state in iPD brains and rat models of PD. Additional studies examined the role of oxidative stress in activating LRRK2, as well as downstream consequences of LRRK2 activity *in vivo*.

*CRISPR/Cas9 Genome Editing of HEK293 Cells to Produce LRRK2 Knockout and Knock-in Cell Lines.* To generate a LRRK2 knockout cell line, a CRISPR/Cas9 genome editing approach was used. A gRNA targeting exon 41 of the LRRK2 gene (5'- ATTGCAAAGATTGCTGACTAGTTTT- 3') was cloned into the GeneArt CRISPR Nuclease vector (Invitrogen) as described by the manufacturer. HEK293 cells were transfected by nucleoporation using a Nucleoporater II device (Amaxa). Transfected cells were collected and enriched by FACS sorting. Sorted cells were grown and expanded for PCR and DNA sequencing analyses. To confirm gene editing of the LRRK2 gene, a region of exon 41 was PCR amplified using a forward primer (5'-TTTAAGGGACAAAGTGAGCA-3') and reverse primer (5'-CACAATGTGATGCTTGCATTT-3') and the resulting PCR product was sequenced. The LRRK2 G2019S knock-in cell line was generated using a similar approach but included transfection of a 120-mer single-stranded oligonucleotide containing a G to A substitution coding for a glycine to serine amino acid change.

A SNCA knockout cell line was generated using a similar approach but utilized a gRNA targeting exon 4 of the α-synuclein (SNCA) gene (5'-CTTTGTCAAAAAGGACCAGT-3') To confirm gene editing of the SNCA gene, a region of exon 4 was PCR amplified using a forward primer (5'- CCACCCTTTAATCTGTTGTTGC-3')

and reverse primer (5'- ATATAAAGGTAGCACTTTTTCACAAGG-3') and the resulting PCR product was sequenced.

*Proximity Ligation Assay*. PLA was performed as described previously in 4% PFA-fixed tissue or cells (*15*). Samples were incubated with specific primary antibodies to the proteins to be detected. Secondary antibodies conjugated with oligonucleotides were added to the reaction and incubated. Ligation solution, consisting of two oligonucleotides and ligase, was added. In this assay, the oligonucleotides hybridize to the two PLA probes and join to a closed loop if they are in close proximity. Amplification solution, consisting of nucleotides and fluorescently labeled oligonucleotides, was added together with polymerase. The oligonucleotide arm of one of the PLA probes acts as a primer for "rolling-circle amplification" using the ligated circle as a template, and this generates a concatemeric product. Fluorescently labeled oligonucleotides hybridize to the RCA product. The PL signal was visible as a distinct fluorescent spot and was analyzed by confocal microscopy (Duolink; Sigma Aldrich). Control experiments included routine immunofluorescence staining of the proteins of interest under identical experimental conditions.

*Statistical analyses*. Each result presented here was derived from 3-6 independent experiments. For simple comparisons of 2 experimental conditions, 2-tailed, unpaired t-tests were used. Where variances were not equal, Welch's correction was used. When virus was injected into 1 hemisphere of the brain and the other hemisphere was used as a control, 2-tailed paired t-tests. For comparisons of multiple experimental conditions, 1-way or 2-way ANOVA was used, and if significant overall, post hoc corrections (Bonferroni or Sidak) for multiple pairwise comparisons were made. P-values less than 0.05 were considered significant.

Other methods are described in **Supplemental Materials**.

**LIST OF SUPPLEMENTARY MATERIALS**

**REFERENCES AND NOTES**


1. L. V. Kalia, A. E. Lang, Parkinson disease in 2015: Evolving basic, pathological and clinical concepts in PD. *Nat Rev Neurol* **12**, 65-66 (2016).

2. C. Paisan-Ruiz, S. Jain, E. W. Evans, W. P. Gilks, J. Simon, M. van der Brug, A. Lopez de Munain, S. Aparicio, A. M. Gil, N. Khan, J. Johnson, J. R. Martinez, D. Nicholl, I. M. Carrera, A. S. Pena, R. de Silva, A. Lees, J. F. Marti-Masso, J. Perez-Tur, N. W. Wood, A. B. Singleton, Cloning of the gene containing mutations that cause PARK8-linked Parkinson's disease. *Neuron* **44**, 595-600 (2004).

3. A. Zimprich, S. Biskup, P. Leitner, P. Lichtner, M. Farrer, S. Lincoln, J. Kachergus, M. Hulihan, R. J. Uitti, D. B. Calne, A. J. Stoessl, R. F. Pfeiffer, N. Patenge, I. C. Carbajal, P. Vieregge, F. Asmus, B. Muller-Myhsok, D. W. Dickson, T. Meitinger, T. M. Strom, Z. K. Wszolek, T. Gasser, Mutations in LRRK2 cause autosomal-dominant parkinsonism with pleomorphic pathology. *Neuron* **44**, 601-607 (2004).

4. J. Simon-Sanchez, C. Schulte, J. M. Bras, M. Sharma, J. R. Gibbs, D. Berg, C. Paisan-Ruiz, P. Lichtner, S. W. Scholz, D. G. Hernandez, R. Kruger, M. Federoff, C. Klein, A. Goate, J. Perlmutter, M. Bonin, M. A. Nalls, T. Illig, C. Gieger, H. Houlden, M. Steffens, M. S. Okun, B. A. Racette, M. R. Cookson, K. D. Foote, H. H. Fernandez, B. J. Traynor, S. Schreiber, S. Arepalli, R. Zonozi, K. Gwinn, M. van der Brug, G. Lopez, S. J. Chanock, A. Schatzkin, Y. Park, A. Hollenbeck, J. Gao, X. Huang, N. W. Wood, D. Lorenz, G. Deuschl, H. Chen, O. Riess, J. A. Hardy, A. B. Singleton, T. Gasser, Genome-wide association study reveals genetic risk underlying Parkinson's disease. *Nat Genet* **41**, 1308-1312 (2009).

5. E. Greggio, S. Jain, A. Kingsbury, R. Bandopadhyay, P. Lewis, A. Kaganovich, M. P. van der Brug, A. Beilina, J. Blackinton, K. J. Thomas, R. Ahmad, D. W. Miller, S. Kesavapany, A. Singleton, A. Lees, R. J. Harvey, K. Harvey, M. R. Cookson, Kinase activity is required for the toxic effects of mutant LRRK2/dardarin. *Neurobiol Dis* **23**, 329-341 (2006).

6. M. Steger, F. Tonelli, G. Ito, P. Davies, M. Trost, M. Vetter, S. Wachter, E. Lorentzen, G. Duddy, S. Wilson, M. A. Baptista, B. K. Fiske, M. J. Fell, J. A. Morrow, A. D. Reith, D. R. Alessi, M. Mann, Phosphoproteomics reveals that Parkinson's disease kinase LRRK2 regulates a subset of Rab GTPases. *eLife* **5**, (2016).

7. K. B. Fraser, A. B. Rawlins, R. G. Clark, R. N. Alcalay, D. G. Standaert, N. Liu, C. Parkinson's Disease Biomarker Program, A. B. West, Ser(P)-1292 LRRK2 in urinary exosomes is elevated in idiopathic Parkinson's disease. *Mov Disord* **31**, 1543-1550 (2016).

8. Z. Sheng, S. Zhang, D. Bustos, T. Kleinheinz, C. E. Le Pichon, S. L. Dominguez, H. O. Solanoy, J. Drummond, X. Zhang, X. Ding, F. Cai, Q. Song, X. Li, Z. Yue, M. P. van der Brug, D. J. Burdick, J. Gunzner-Toste, H. Chen, X. Liu, A. A. Estrada, Z. K. Sweeney, K. Scearce-Levie, J. G. Moffat, D. S. Kirkpatrick, H. Zhu, Ser1292 autophosphorylation is an indicator of LRRK2 kinase activity and contributes to the cellular effects of PD mutations. *Sci Transl Med* **4**, 164ra161 (2012).

9. X. Li, Q. J. Wang, N. Pan, S. Lee, Y. Zhao, B. T. Chait, Z. Yue, Phosphorylation-dependent 14-3-3 binding to LRRK2 is impaired by common mutations of familial Parkinson's disease. *PLoS One* **6**, e17153 (2011).

10. N. Dzamko, M. Deak, F. Hentati, A. D. Reith, A. R. Prescott, D. R. Alessi, R. J. Nichols, Inhibition of LRRK2 kinase activity leads to dephosphorylation of Ser(910)/Ser(935), disruption of 14-3-3 binding and altered cytoplasmic localization. *Biochem J* **430**, 405-413 (2010).

11. N. J. Lavalley, S. R. Slone, H. Ding, A. B. West, T. A. Yacoubian, 14-3-3 Proteins regulate mutant LRRK2 kinase activity and neurite shortening. *Hum Mol Genet* **25**, 109-122 (2016).

12. A. Mamais, R. Chia, A. Beilina, D. N. Hauser, C. Hall, P. A. Lewis, M. R. Cookson, R. Bandopadhyay, Arsenite stress down-regulates phosphorylation and 14-3-3 binding of leucine-rich repeat kinase 2 (LRRK2), promoting self-association and cellular redistribution. *J Biol Chem* **289**, 21386-21400 (2014).

13. M. J. Fell, C. Mirescu, K. Basu, B. Cheewatrakoolpong, D. E. DeMong, J. M. Ellis, L. A. Hyde, Y. Lin, C. G. Markgraf, H. Mei, M. Miller, F. M. Poulet, J. D. Scott, M. D. Smith, Z. Yin, X. Zhou, E. M. Parker, M. E. Kennedy, J. A. Morrow, MLi-2, a Potent, Selective, and Centrally Active Compound for Exploring the Therapeutic Potential and Safety of LRRK2 Kinase Inhibition. *J Pharmacol Exp Ther* **355**, 397-409 (2015).

14. M. S. Moehle, P. J. Webber, T. Tse, N. Sukar, D. G. Standaert, T. M. DeSilva, R. M. Cowell, A. B. West, LRRK2 inhibition attenuates microglial inflammatory responses. *J Neurosci* **32**, 1602-1611 (2012).

15. R. Di Maio, P. J. Barrett, E. K. Hoffman, C. W. Barrett, A. Zharikov, A. Borah, X. Hu, J. McCoy, C. T. Chu, E. A. Burton, T. G. Hastings, J. T. Greenamyre, alpha-Synuclein binds to TOM20 and inhibits mitochondrial protein import in Parkinson's disease. *Sci Transl Med* **8**, 342ra378 (2016).

16. J. T. Greenamyre, J. R. Cannon, R. Drolet, P. G. Mastroberardino, Lessons from the rotenone model of Parkinson's disease. *Trends Pharmacol Sci* **31**, 141-142; author reply 142-143 (2010).

17. A. Ulusoy, M. Decressac, D. Kirik, A. Bjorklund, Viral vector-mediated overexpression of alpha-synuclein as a progressive model of Parkinson's disease. *Prog Brain Res* **184**, 89-111 (2010).

18. H. Dimant, S. K. Kalia, L. V. Kalia, L. N. Zhu, L. Kibuuka, D. Ebrahimi-Fakhari, N. R. McFarland, Z. Fan, B. T. Hyman, P. J. McLean, Direct detection of alpha synuclein oligomers in vivo. *Acta neuropathologica communications* **1**, 6 (2013).

19. R. Betarbet, R. M. Canet-Aviles, T. B. Sherer, P. G. Mastroberardino, C. McLendon, J. H. Kim, S. Lund, H. M. Na, G. Taylor, N. F. Bence, R. Kopito, B. B. Seo, T. Yagi, A. Yagi, G. Klinefelter, M. R. Cookson, J. T. Greenamyre, Intersecting pathways to neurodegeneration in Parkinson's disease: effects of the pesticide rotenone on DJ-1, alpha-synuclein, and the ubiquitin-proteasome system. *Neurobiol Dis* **22**, 404-420 (2006).

20. R. R. Nazarewicz, A. E. Dikalova, A. Bikineyeva, S. I. Dikalov, Nox2 as a potential target of mitochondrial superoxide and its role in endothelial oxidative stress. *Am J Physiol Heart Circ Physiol* **305**, H1131-1140 (2013).

21. S. I. Dikalov, W. Li, A. K. Doughan, R. R. Blanco, A. M. Zafari, Mitochondrial reactive oxygen species and calcium uptake regulate activation of phagocytic NADPH oxidase. *Am J Physiol Regul Integr Comp Physiol* **302**, R1134-1142 (2012).

22. G. Csanyi, E. Cifuentes-Pagano, I. Al Ghouleh, D. J. Ranayhossaini, L. Egana, L. R. Lopes, H. M. Jackson, E. E. Kelley, P. J. Pagano, Nox2 B-loop peptide, Nox2ds, specifically inhibits the NADPH oxidase Nox2. *Free Radic Biol Med* **51**, 1116-1125 (2011).

23. K. Thirstrup, J. C. Dachsel, F. S. Oppermann, D. S. Williamson, G. P. Smith, K. Fog, K. V. Christensen, Selective LRRK2 kinase inhibition reduces phosphorylation of endogenous Rab10 and Rab12 in human peripheral mononuclear blood cells. *Scientific reports* **7**, 10300 (2017).

24. M. Baptista, K. M. Merchant, S. Bharghava, D. Bryce, M. Ellis, A. A. Estrada, M. J. Fell, R. Fuji, P. Galatsis, S. Hill, W. D. Hirst, C. Houle, M. Kennedy, X. Liu, M. Maddess, C. G. Markgraf, H. Mei, E. Needle, S. J. Steyn, Z. Yin, H. Yu, B. Fiske, T. B. Sherer, LRRK2 kinase inhibitors of different structural classes induce abnormal, but reversible, accumulation of lamellar bodies in type II pneumocytes in non-human primates. Program No. 763.02. *2015 Neuroscience Meeting Planner. Washington, DC: Society for Neuroscience, 2015. Online.*, (2015).

25. A. Kleinknecht, B. Popova, D. F. Lazaro, R. Pinho, O. Valerius, T. F. Outeiro, G. H. Braus, C-Terminal Tyrosine Residue Modifications Modulate the Protective Phosphorylation of Serine

129 of alpha-Synuclein in a Yeast Model of Parkinson's Disease. *PLoS Genet* **12**, e1006098 (2016).

26. A. Oueslati, B. L. Schneider, P. Aebischer, H. A. Lashuel, Polo-like kinase 2 regulates selective autophagic alpha-synuclein clearance and suppresses its toxicity in vivo. *Proc Natl Acad Sci U S A* **110**, E3945-3954 (2013).

27. A. M. Cuervo, L. Stefanis, R. Fredenburg, P. T. Lansbury, D. Sulzer, Impaired degradation of mutant alpha-synuclein by chaperone-mediated autophagy. *Science* **305**, 1292-1295 (2004).

28. J. L. Webb, B. Ravikumar, J. Atkins, J. N. Skepper, D. C. Rubinsztein, Alpha-Synuclein is degraded by both autophagy and the proteasome. *J Biol Chem* **278**, 25009-25013 (2003).

29. J. P. Daher, H. A. Abdelmotilib, X. Hu, L. A. Volpicelli-Daley, M. S. Moehle, K. B. Fraser, E. Needle, Y. Chen, S. J. Steyn, P. Galatsis, W. D. Hirst, A. B. West, Leucine-rich Repeat Kinase 2 (LRRK2) Pharmacological Inhibition Abates alpha-Synuclein Gene-induced Neurodegeneration. *J Biol Chem* **290**, 19433-19444 (2015).

30. J. P. Daher, L. A. Volpicelli-Daley, J. P. Blackburn, M. S. Moehle, A. B. West, Abrogation of alpha-synuclein-mediated dopaminergic neurodegeneration in LRRK2-deficient rats. *Proc Natl Acad Sci U S A* **111**, 9289-9294 (2014).

31. X. Li, D. J. Moore, Y. Xiong, T. M. Dawson, V. L. Dawson, Reevaluation of phosphorylation sites in the Parkinson disease-associated leucine-rich repeat kinase 2. *J Biol Chem* **285**, 29569-29576 (2010).

32. Z. Li, R. J. Schulze, S. G. Weller, E. W. Krueger, M. B. Schott, X. Zhang, C. A. Casey, J. Liu, J. Stockli, D. E. James, M. A. McNiven, A novel Rab10-EHBP1-EHD2 complex essential for the autophagic engulfment of lipid droplets. *Sci Adv* **2**, e1601470 (2016).

33. O. V. Vieira, Rab3a and Rab10 are regulators of lysosome exocytosis and plasma membrane repair. *Small GTPases*, 1-3 (2016).

34. A. R. English, G. K. Voeltz, Rab10 GTPase regulates ER dynamics and morphology. *Nat Cell Biol* **15**, 169-178 (2013).

35. L. A. Volpicelli-Daley, H. Abdelmotilib, Z. Liu, L. Stoyka, J. P. Daher, A. J. Milnerwood, V. K. Unni, W. D. Hirst, Z. Yue, H. T. Zhao, K. Fraser, R. E. Kennedy, A. B. West, G2019S-LRRK2 Expression Augments alpha-Synuclein Sequestration into Inclusions in Neurons. *J Neurosci* **36**, 7415-7427 (2016).

36. L. H. Sanders, J. McCoy, X. Hu, P. G. Mastroberardino, B. C. Dickinson, C. J. Chang, C. T. Chu, B. Van Houten, J. T. Greenamyre, Mitochondrial DNA damage: Molecular marker of vulnerable nigral neurons in Parkinson's disease. *Neurobiol Dis* **70**, 214-223 (2014).

37. A. D. Zharikov, J. R. Cannon, V. Tapias, Q. Bai, M. P. Horowitz, V. Shah, A. El Ayadi, T. G. Hastings, J. T. Greenamyre, E. A. Burton, shRNA targeting alpha-synuclein prevents neurodegeneration in a Parkinson's disease model. *J Clin Invest* **125**, 2721-2735 (2015).

38. I. Alafuzoff, P. G. Ince, T. Arzberger, S. Al-Sarraj, J. Bell, I. Bodi, N. Bogdanovic, O. Bugiani, I. Ferrer, E. Gelpi, S. Gentleman, G. Giaccone, J. W. Ironside, N. Kavantzas, A. King, P. Korkolopoulou, G. G. Kovacs, D. Meyronet, C. Monoranu, P. Parchi, L. Parkkinen, E. Patsouris, W. Roggendorf, A. Rozemuller, C. Stadelmann-Nessler, N. Streichenberger, D. R. Thal, H. Kretzschmar, Staging/typing of Lewy body related alpha-synuclein pathology: a study of the BrainNet Europe Consortium. *Acta Neuropathol* **117**, 635-652 (2009).

39. ***Acknowledgements:*** This work was supported by research grants from the National Institutes of Health (NS100744, R21ES027470, NS095387, AG005133), the Blechman Foundation, the American Parkinson Disease Association, and friends and family of Sean Logan. The brain bank has received support from the University of Pittsburgh Brain Institute. Work in the Alessi lab on LRRK2 is supported by the Michael J. Fox Foundation for Parkinson's research [grant number 6986]; the Medical Research Council [grant number MC_UU_12016/2] and the pharmaceutical companies supporting the Division of Signal Transduction Therapy Unit (Boehringer‐Ingelheim, GlaxoSmithKline, and Merck KGaA, to D.R.A.). Competing interests: Greenamyre briefly held an advisory position at Pfizer. Otherwise, the authors declare that they have no competing financial interests. Data and Materials Availability: JTG received the PF-360 compound from Pfizer and is not authorized to distribute it.

**Figure Legends**

***Figure 1.*** Validation of assays using CRISPR/Cas9 gene-edited cells and selective LRRK2 kinase inhibitors. **(A)** PL assay showing LRRK2 kinase activation by means of phosphorylation of the autophosphorylation site, Ser1292 (red signal) and immunofluorescence of phosphorylation of the LRRK2 substrate Rab10 (green signal). In WT HEK cells (top row), there was little PL signal or pThr73-Rab10 immunofluorescence. In HEK$^{G2019S/G2019S}$ cells (2$^{nd}$ row) with elevated LRRK2 kinase activity, there was a bright pS1292 PL signal and strong pThr73-Rab immunofluorescence. In LRRK2 knockout HEK cells (bottom row) there was no pS1292 PL signal and very little pThr73-Rab signal. **(B)** Quantification of the pS1292 PL signal in WT, G2019S and knockout cells. Results reflect 3 independent experiments. Each symbol represents signal from a single cell. Statistical testing by ANOVA with post hoc Bonferroni correction. **(C)** Quantification of the pThr73-Rab10 signal in WT, G2019S and knockout cells. Results reflect 3 independent experiments. Each symbol represents signal from a single cell. Statistical testing by ANOVA with post hoc Bonferroni correction. **(D)** PL assay of 14-3-3 binding to LRRK2 and immunofluorescence of Rab10 phosphorylation at Thr73. In WT cells, there was a strong 14-3-3-LRRK2 PL signal (red) and little pThr73-Rab10 immunofluorescence (green). In HEK$^{G2019S/G2019S}$ cells, there was loss of 14-3-3 binding and a marked increase in pThr73-Rab10 signal. In LRRK2 knockout cells there was no 14-3-3-LRRK2 signal and little pThr73-Rab10 signal. **(E)** Quantification of the 14-3-3-LRRK2 PL signal in WT, G2019S and knockout cells. Results reflect 3 independent experiments. Each symbol represents signal from a single cell. Statistical testing by ANOVA with post hoc Bonferroni correction. **(F)** Dose-response curves of the LRRK2 kinase inhibitor GNE-7915 against the pS1292 PL signal (filled circles) and the pThr73-Rab10 signal (open circles) in HEK$^{G2019S/G2019S}$ cells. Cells were cultured for 24 hours with various inhibitor concentrations. Results from 3 independent experiments. Symbols show mean ± SEM. $IC_{50}$ values calculated by GraphPad Prism software. **(G)** Dose-response curves of the LRRK2 kinase inhibitor MLi-2 against the pS1292 PL signal (filled circles) and the pThr73-Rab10 signal (open circles) in

HEK$^{G2019S/G2019S}$ cells. Cells were cultured for 24 hours with various inhibitor concentrations. **(H)** Dose-response curves of the LRRK2 kinase inhibitor GNE-7915 against the pS1292 PL signal (filled circles) and the pThr73-Rab10 signal (open circles) in LCLs derived from an individual carrying the G2019S mutation. Cells were cultured for 24 hours with various inhibitor concentrations.

***Figure 2.*** Activation of LRRK2 kinase activity in nigrostriatal neurons in iPD. **(A)** pS1292 PL (red) and pThr73-Rab10 (gray) immunofluorescence signals in sections of substantia nigra from a control brain (top row) and a brain from an individual with iPD (bottom row). In the control brain, there was little pS1292 or pThr73-Rab10 signal, but in the iPD brain there were strong signals for both. **(B)** Quantification of pS1292 PL signal in 8 control brains and 7 iPD brains. Statistical comparison by unpaired 2-tail t-test. **(C)** Quantification of pThr73-Rab10 signal in 8 control brains and 7 iPD brains. Statistical comparison by unpaired 2-tail t-test. **(D)** 14-3-3-LRRK2 PL (red) and pThr73-Rab10 (gray) immunofluorescence signals in sections of substantia nigra from a control brain (top row) and a brain from an individual with iPD (bottom row). In the control brain, there was strong 14-3-3-LRRK2 PL signal and little pThr73-Rab10 signal, but in the iPD brain the opposite pattern was seen. **(E)** Quantification of 14-3-3-LRRK2 PL signal in 8 control brains and 7 iPD brains. Statistical comparison by unpaired 2-tail t-test.

***Figure 3.*** Nigrostriatal LRRK2 activation is reproduced in 2 rat models of PD. **(A)** pS1292 PL and 14-3-3-LRRK2 PL signals in substantia nigra of control and rotenone treated rats. In the rotenone rats, there was increased pS1292 PL and loss of 14-3-3-LRRK2 PL signal indicating LRRK2 activation. **(B)** Quantification of pS1292 PL signal in nigrostriatal dopamine neurons from control and rotenone treated rats. Symbols represent individual animals. Statistical comparison by unpaired 2-tail t-test. **(C)** Quantification of 14-3-3-LRRK2 PL signal in nigrostriatal dopamine neurons from control and rotenone

treated rats. Symbols represent individual animals. Statistical comparison by unpaired 2-tail t-test. **(D)** pS1292 PL and 14-3-3-LRRK2 PL signals in substantia nigra of rats that received a unilateral injection of AAV2-*hSNCA*. In the hemisphere overexpressing α-synuclein, there was increased pS1292 PL and loss of 14-3-3-LRRK2 PL signal indicating LRRK2 activation in nigrostriatal neurons. **(E)** Quantification of pS1292 PL signal in nigrostriatal dopamine neurons from the control and AAV-*hSNCA* injected hemispheres. Symbols represent mean values from each hemisphere. Statistical comparison by paired 2-tail t-test. **(F)** Quantification of 14-3-3-LRRK2 PL signal in nigrostriatal dopamine neurons from the control and AAV-hSNCA injected hemispheres. Symbols represent mean values from each hemisphere. Statistical comparison by paired 2-tail t-test.

***Figure 4.*** LRRK2 is activated by reactive oxygen species. **(A)** pS1292 PL signal is increased dose-dependently by $H_2O_2$ (blue symbols), and the $H_2O_2$-induced increase is blocked by the antioxidant α-tocopherol (5 μM) (red symbols). Results represent 3 independent experiments. Symbols represent measurements from individual cells. Red asterisks = $p<0.0001$ vs no $H_2O_2$, ANOVA with Bonferroni correction; blue asterisks = $p<0.0001$ vs $H_2O_2$ alone at the same concentration. **(B)** pThr73-Rab10 signal is increased dose-dependently by $H_2O_2$ (blue symbols), and the $H_2O_2$-induced increase is blocked by the antioxidant α-tocopherol (5 μM) (red symbols). Results represent 3 independent experiments. Symbols represent measurements from individual cells. Red asterisks = $p<0.0001$ vs no $H_2O_2$, ANOVA with Bonferroni correction; blue asterisks = $p<0.0001$ vs $H_2O_2$ alone at the same concentration. ns = not significant. **(C)** In WT HEK cells rotenone treatment activates pS1292 signal and pThr73-Rab10 immunoreactivity. Both effects are blocked by the specific NOX2 inhibitor Nox2ds-tat. **(D)** Quantification of the pS1292 PL signal in vehicle- and rotenone-treated cells. Results represent 3 independent experiments. Symbols represent measurements from individual cells. Comparison by ANOVA with Bonferroni correction. **(E)** Quantification of the pThr73-Rab10 immunofluorescent signal

in vehicle- and rotenone-treated cells. Results represent 3 independent experiments. Symbols represent measurements from individual cells. Comparison by ANOVA with Bonferroni correction.

***Figure 5.*** Nigrostriatal LRRK2 activation and pSer129-α-synuclein accumulation can be blocked *in vivo* by a brain penetrant LRRK2 kinase inhibitor. **(A)** pS1292 PL and pThr73-Rab10 signals in rats treated with vehicle, PF-360 alone, rotenone alone and rotenone + PF-360. **(B)** Quantification of pS1292 PL signal in rats treated with vehicle, PF-360 alone, rotenone alone and rotenone + PF-360. Symbols represent individual rats. Comparison by ANOVA with Bonferroni correction. **(C)** Quantification of pThr73-Rab10 signal in rats treated with vehicle, PF-360 alone, rotenone alone and rotenone + PF-360. Symbols represent individual rats. Comparison by ANOVA with Bonferroni correction. **(D)** pSer129-α-Synuclein immunoreactivity in rats treated with vehicle, PF-360 alone, rotenone alone and rotenone + PF-360. **(E)** Quantification of pSer129-α-synuclein signal in rats treated with vehicle, PF-360 alone, rotenone alone and rotenone + PF-360. Symbols represent individual rats. Comparison by ANOVA with Bonferroni correction.

***Figure 6.*** Rotenone induces *in vivo* nigrostriatal lysosomal and CMA defects that are prevented by co-treatment with a LRRK2 kinase inhibitor. **(A)** Nigrostriatal Lamp1 and p62/SQSTM1 immunoreactivity in rats treated with vehicle, PF-360 alone, rotenone alone and rotenone + PF-360. **(B)** Nigrostriatal Lamp2A immunoreactivity in rats treated with vehicle, PF-360 alone, rotenone alone and rotenone + PF-360. **(C)** Quantification of Lamp1 signal in rats treated with vehicle, PF-360 alone, rotenone alone and rotenone + PF-360. Symbols represent individual rats. Comparison by ANOVA with Bonferroni correction. **(D)** Quantification of p62/SQSTM1 signal in rats treated with vehicle, PF-360 alone, rotenone alone and rotenone + PF-360. Symbols represent individual rats. Comparison by ANOVA with Bonferroni correction. **(E)** Quantification of Lamp2A signal in rats treated with vehicle, PF-360 alone,

rotenone alone and rotenone + PF-360. Symbols represent individual rats. Comparison by ANOVA with Bonferroni correction. **(F)** Substantia nigra Lamp1 and p62/SQSTM1 immunoreactivity in a control brain and 2 iPD brains. In controls, dopamine neurons contain many small punctae of Lamp1 immunoreactivity and very little detectable p62/SQSTM1, presumably reflecting efficient autophagic flux. In iPD brains, note the marked loss of Lamp1 and accumulation of p62/SQSTM1 into large inclusions (Lewy bodies) in dopamine neurons in the iPD brains. **(G)** Quantification of Lamp1 in control vs iPD dopamine neurons. Symbols represent individual brains. Comparison by unpaired 2-tail t-test. **(H)** Quantification of Lamp1 in control vs iPD dopamine neurons. Symbols represent individual brains. Comparison by unpaired 2-tail t-test.

***Figure 7.*** Accumulated pSer129-α-synuclein binds to TOM20 in iPD and this is replicated in the rotenone rat model and is prevented by co-treatment with a LRRK2 kinase inhibitor. **(A)** pSer129-α-synuclein- (pS129syn)-TOM20 PL signal in human control and iPD substantia nigra brain sections. **(B)** Quantification of the pS129syn-TOM20 PL signal in 8 control brains and 7 iPD brains. Comparison by unpaired 2-tail t-test. **(C)** pS129syn-TOM20 PL signal and Ndufs3 immunoreactivity in substantia nigra of rats treated with vehicle, PF-360 alone, rotenone alone and rotenone + PF-360. In rotenone treated rats there is increased pS129syn-TOM20 PL signal and reduced levels and diffuse redistribution of the nuclear encoded and imported complex I subunit, Ndufs3. These abnormalities were prevented by treatment with PF-360. **(D)** Quantification of the pS129syn-TOM20 PL signal in substantia nigra of rats treated with vehicle, PF-360 alone, rotenone alone and rotenone + PF-360. Symbols represent individual rats. Comparison by ANOVA with Bonferroni correction. **(E)** Graphical representation of the distribution and fluorescence intensity levels of Ndufs3 in nigral dopamine neurons in rats treated with vehicle, PF-360 alone, rotenone alone and rotenone + PF-360. Note the loss of punctate, high intensity staining in the rotenone animals that is preserved by co-treatment with PF-360.

***Figure 8.*** Activation of LRRK2 kinase activity in iPD and its downstream consequences. Our data suggest that most wildtype endogenous LRRK2 is normally in an inactive state bound to 14-3-3 protein (although the specific isoform(s) of 14-3-3 have not been defined here). ROS signaling activates LRRK2 as indicated by phosphorylation of serine 1292 and dissociation from 14-3-3. In turn, LRRK2 kinase activity phosphorylates Rab10 at threonine 73 and inhibits its function by preventing binding to Rab GDP-dissociation inhibitor factors necessary for membrane delivery and recycling. As a result, there is impairment of endosomal and lysosomal function, which leads to accumulation of pSer129-α-synuclein, a known inhibitor of mitochondrial protein import. Blockade of mitochondrial protein import leads to senescent mitochondria that produce more ROS that can feed forward to amplify this cycle. LRRK2 kinase inhibitors block the downstream effects of LRRK2 activation.

***Figure 1***

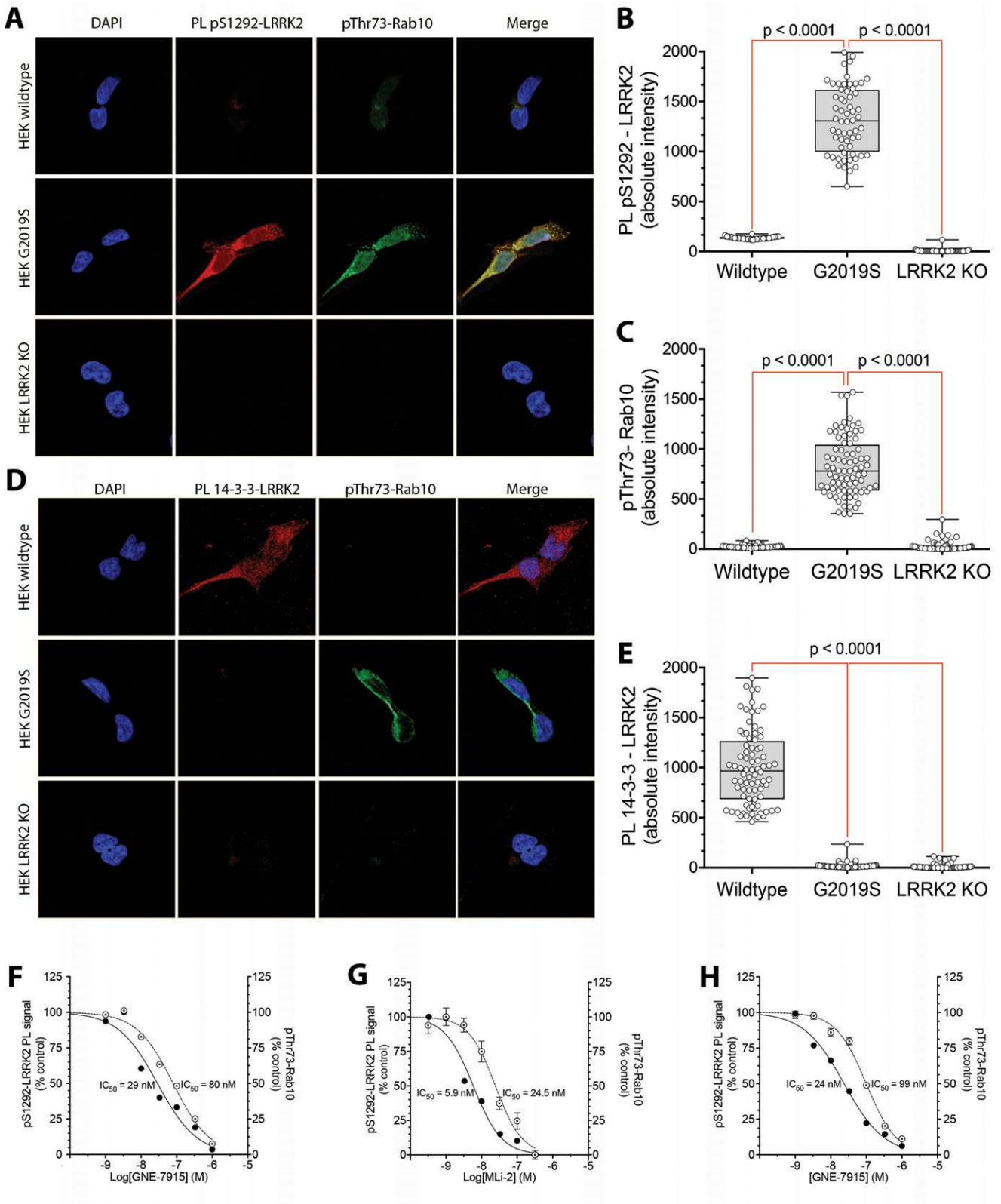
A
DAPI
PL pS1292-LRRK2
pThr73-Rab10
Merge
HEK wildtype
HEK G2019S
HEK LRRK2 KO
B
p < 0.0001
p < 0.0001
PL pS1292 - LRRK2 (absolute intensity)
Wildtype
G2019S
LRRK2 KO
C
pThr73- Rab10 (absolute intensity)
D
PL 14-3-3-LRRK2
E
PL 14-3-3 - LRRK2 (absolute intensity)
F
pS1292-LRRK2 PL signal (% control)
pThr73-Rab10 (% control)
IC50 = 29 nM
IC50 = 80 nM
Log[GNE-7915] (M)
G
IC50 = 5.9 nM
IC50 = 24.5 nM
Log[MLi-2] (M)
H
IC50 = 24 nM
IC50 = 99 nM
[GNE-7915] (M)

***Figure 2***

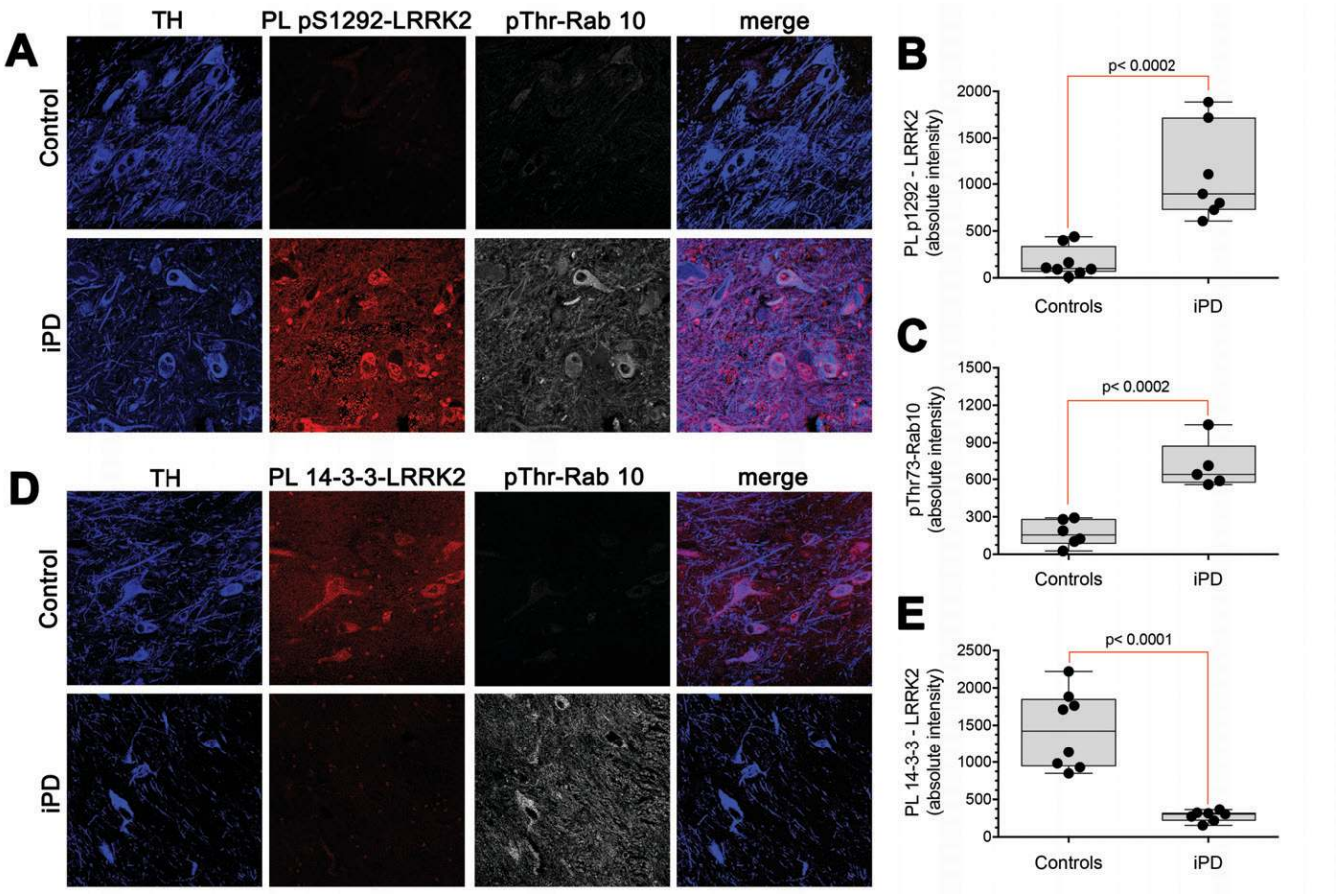
A
TH
PL pS1292-LRRK2
pThr-Rab 10
merge
Control
iPD
B
p< 0.0002
PL p1292 - LRRK2 (absolute intensity)
2000
1500
1000
500
0
Controls
iPD
C
p< 0.0002
pThr73-Rab10 (absolute intensity)
1500
1200
900
600
300
0
Controls
iPD
D
TH
PL 14-3-3-LRRK2
pThr-Rab 10
merge
Control
iPD
E
p< 0.0001
PL 14-3-3 - LRRK2 (absolute intensity)
2500
2000
1500
1000
500
0
Controls
iPD

***Figure 3***

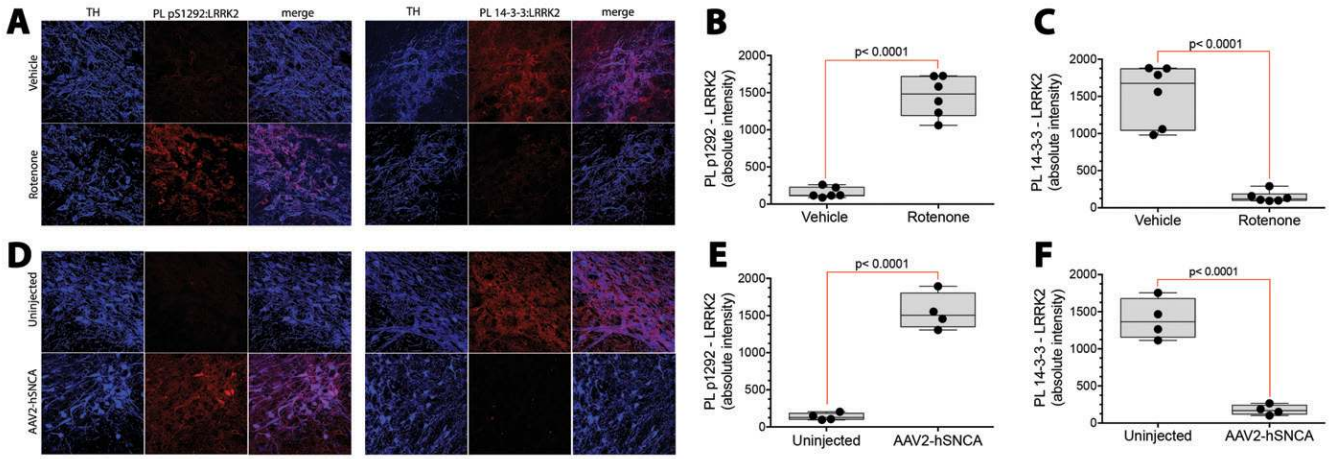
A
TH
PL pS1292:LRRK2
merge
TH
PL 14-3-3:LRRK2
merge
Vehicle
Rotenone
B
p< 0.0001
PL p1292 - LRRK2 (absolute intensity)
2000
1500
1000
500
0
Vehicle
Rotenone
C
p< 0.0001
PL 14-3-3 - LRRK2 (absolute intensity)
2000
1500
1000
500
0
Vehicle
Rotenone
D
Uninjected
AAV2-hSNCA
E
p< 0.0001
PL p1292 - LRRK2 (absolute intensity)
2000
1500
1000
500
0
Uninjected
AAV2-hSNCA
F
p< 0.0001
PL 14-3-3 - LRRK2 (absolute intensity)
2000
1500
1000
500
0
Uninjected
AAV2-hSNCA

*Figure 4*

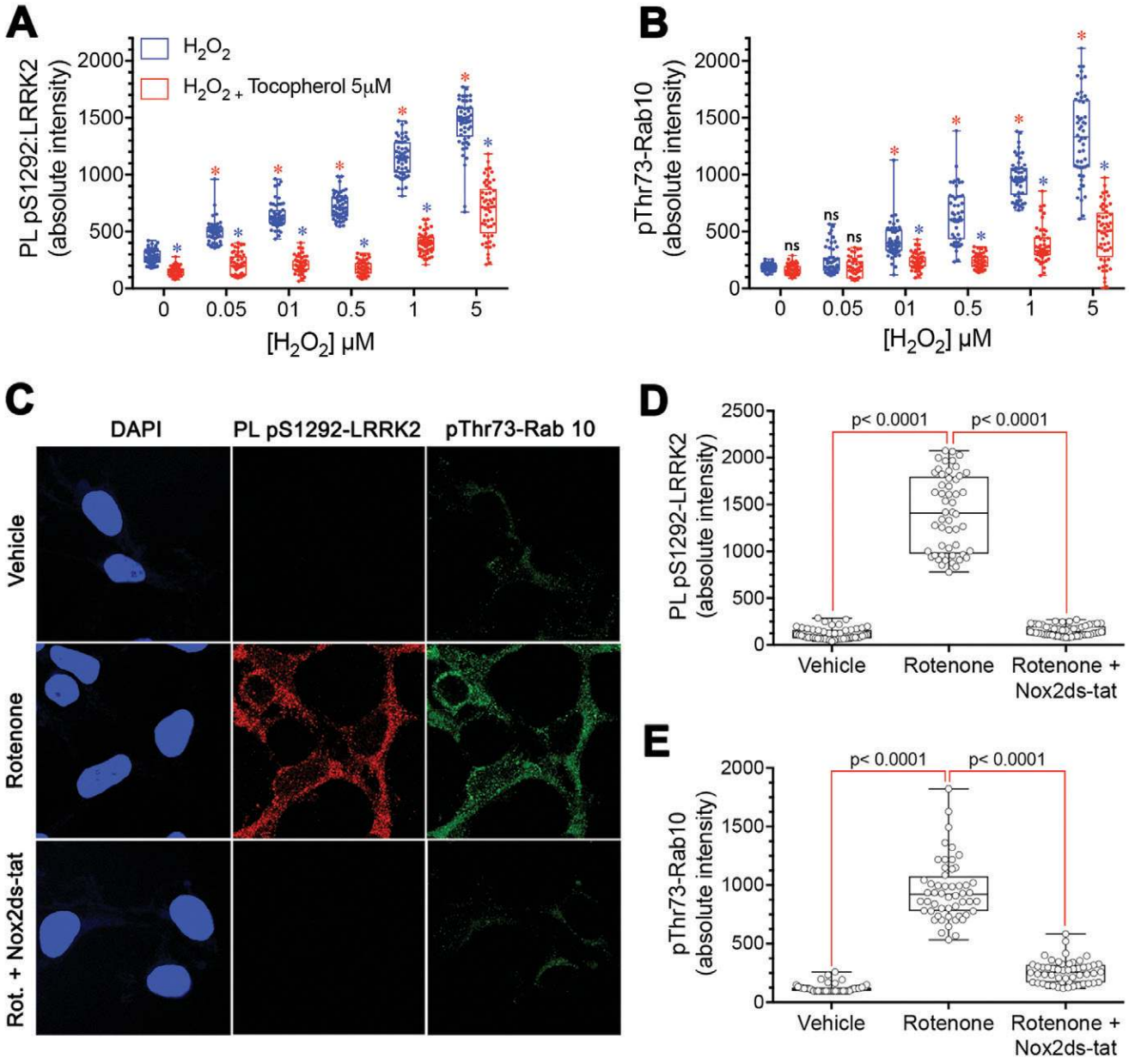
A
PL pS1292:LRRK2 (absolute intensity)
$H_2O_2$
$H_2O_2$ + Tocopherol 5µM
[$H_2O_2$] µM
B
pThr73-Rab10 (absolute intensity)
ns
[$H_2O_2$] µM
C
DAPI
PL pS1292-LRRK2
pThr73-Rab 10
Vehicle
Rotenone
Rot. + Nox2ds-tat
D
PL pS1292-LRRK2 (absolute intensity)
p< 0.0001
p< 0.0001
Vehicle
Rotenone
Rotenone + Nox2ds-tat
E
pThr73-Rab10 (absolute intensity)
p< 0.0001
p< 0.0001
Vehicle
Rotenone
Rotenone + Nox2ds-tat

***Figure 5***

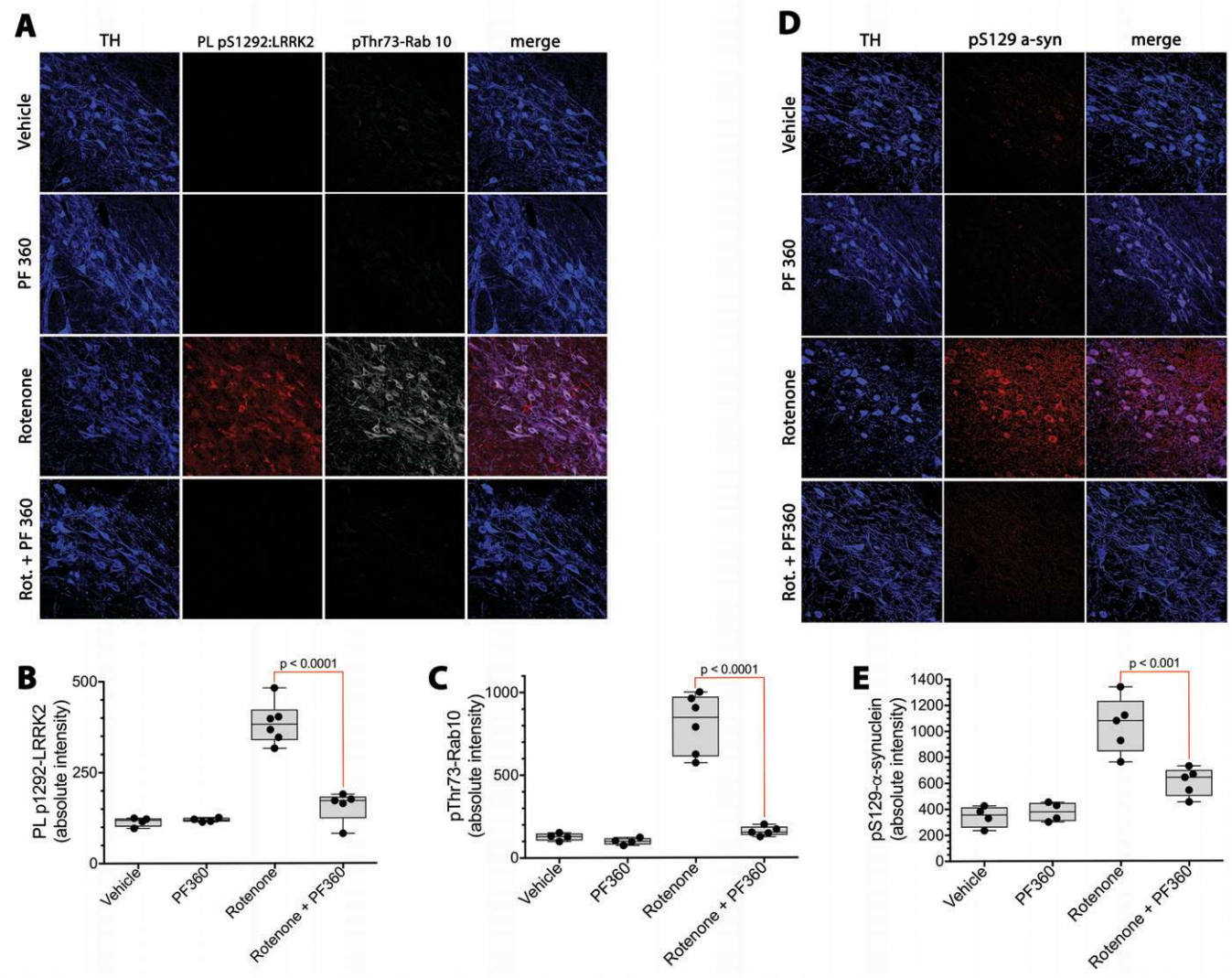
A
TH
PL pS1292:LRRK2
pThr73-Rab 10
merge
Vehicle
PF 360
Rotenone
Rot. + PF 360
D
TH
pS129 a-syn
merge
Vehicle
PF 360
Rotenone
Rot. + PF360
B
PL p1292-LRRK2 (absolute intensity)
p < 0.0001
Vehicle
PF360
Rotenone
Rotenone + PF360
C
pThr73-Rab10 (absolute intensity)
p < 0.0001
Vehicle
PF360
Rotenone
Rotenone + PF360
E
pS129-α-synuclein (absolute intensity)
p < 0.001
Vehicle
PF360
Rotenone
Rotenone + PF360

***Figure 6***

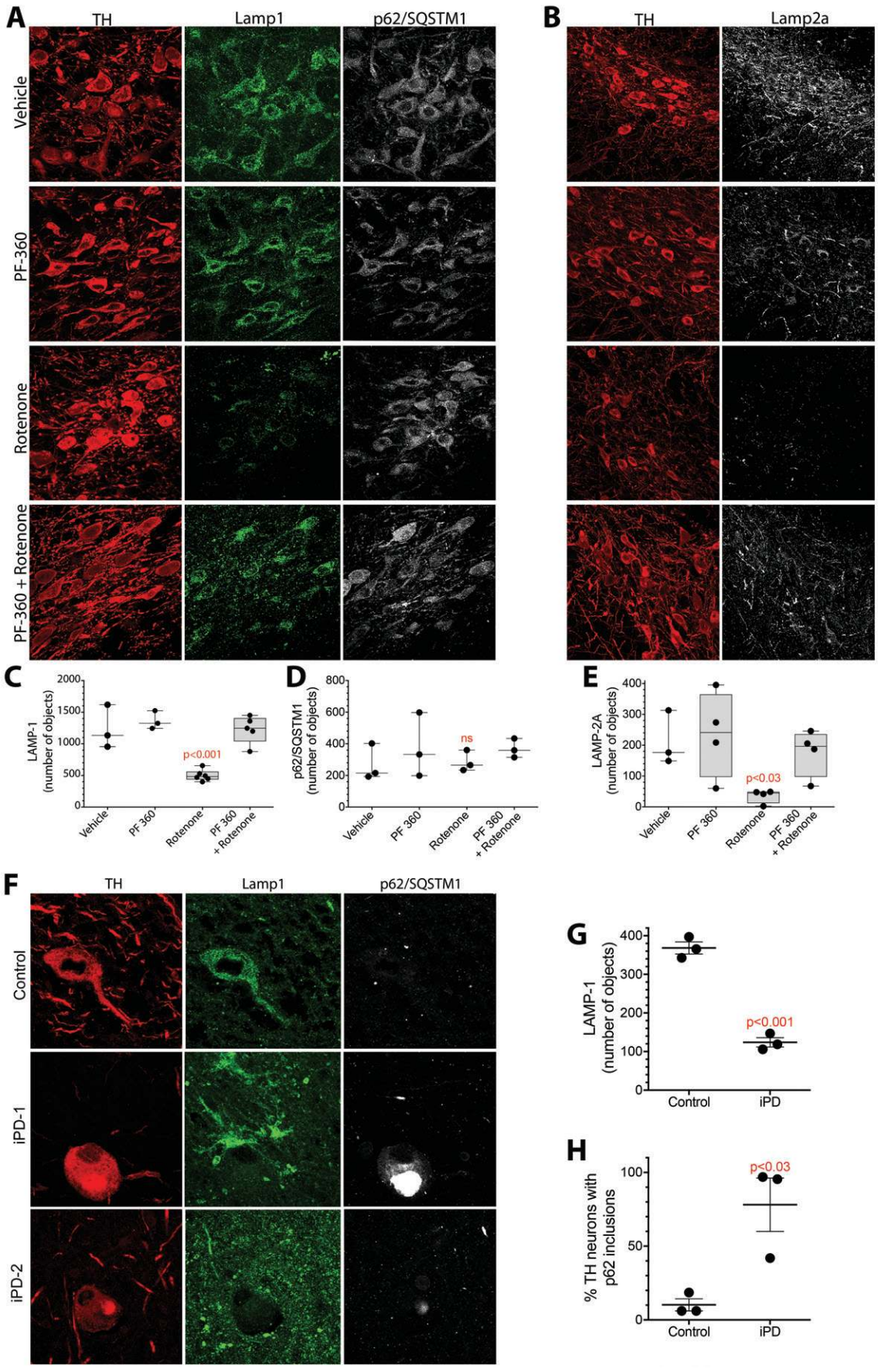
A
TH
Lamp1
p62/SQSTM1
Vehicle
PF-360
Rotenone
PF-360 + Rotenone
B
TH
Lamp2a
C
LAMP-1
(number of objects)
p<0.001
Vehicle
PF 360
Rotenone
PF 360
+Rotenone
D
p62/SQSTM1
(number of objects)
ns
E
LAMP-2A
(number of objects)
p<0.03
F
TH
Lamp1
p62/SQSTM1
Control
iPD-1
iPD-2
G
LAMP-1
(number of objects)
p<0.001
Control
iPD
H
% TH neurons with
p62 inclusions
p<0.03
Control
iPD

***Figure 7***

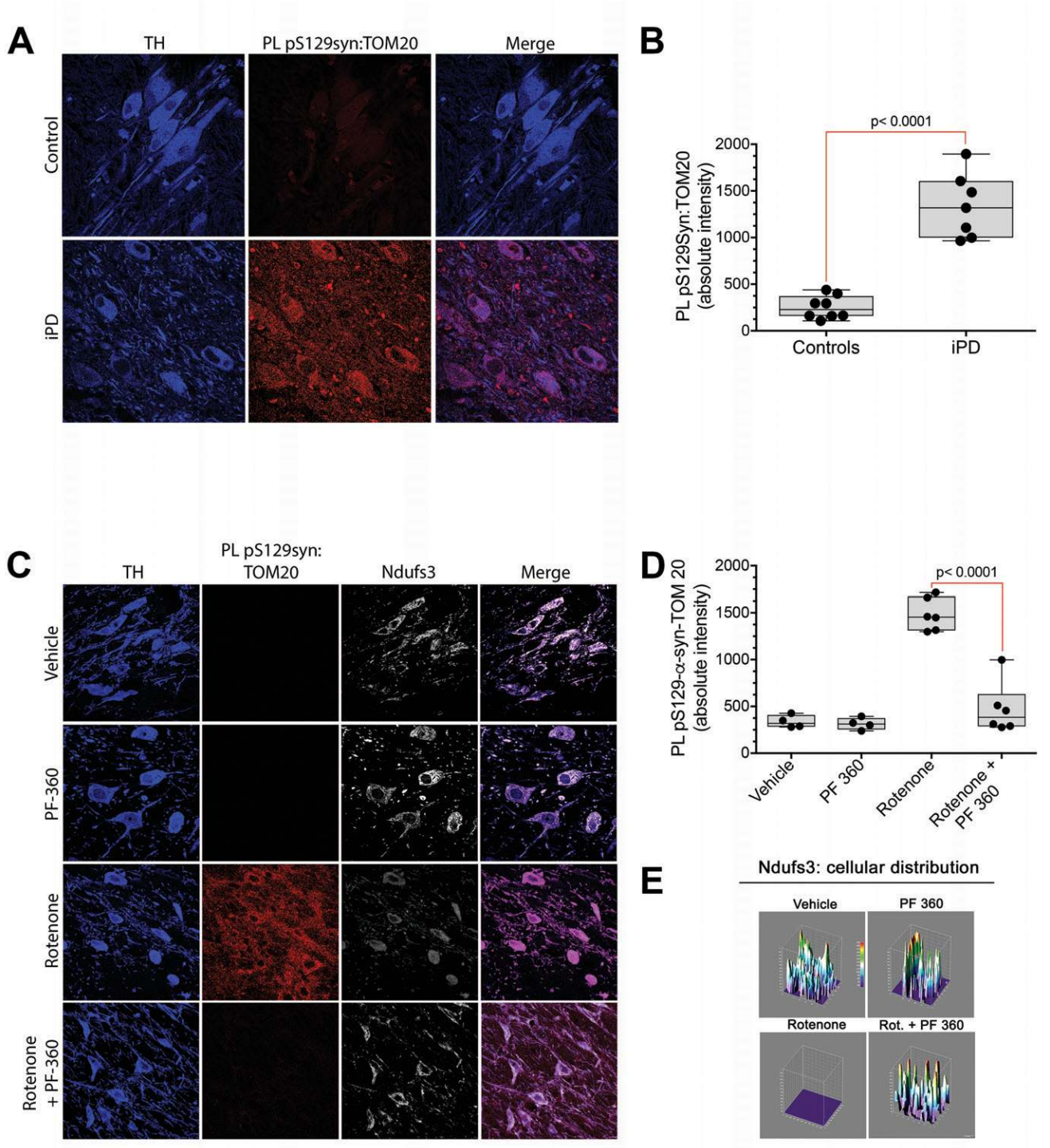
A
TH
PL pS129syn:TOM20
Merge
Control
iPD
B
p< 0.0001
PL pS129Syn:TOM20 (absolute intensity)
2000
1500
1000
500
0
Controls
iPD
C
TH
PL pS129syn: TOM20
Ndufs3
Merge
Vehicle
PF-360
Rotenone
Rotenone + PF-360
D
p< 0.0001
PL pS129-α-syn-TOM 20 (absolute intensity)
2000
1500
1000
500
0
Vehicle
PF 360
Rotenone
Rotenone + PF 360
E
Ndufs3: cellular distribution
Vehicle
PF 360
Rotenone
Rot. + PF 360

***Figure 8***

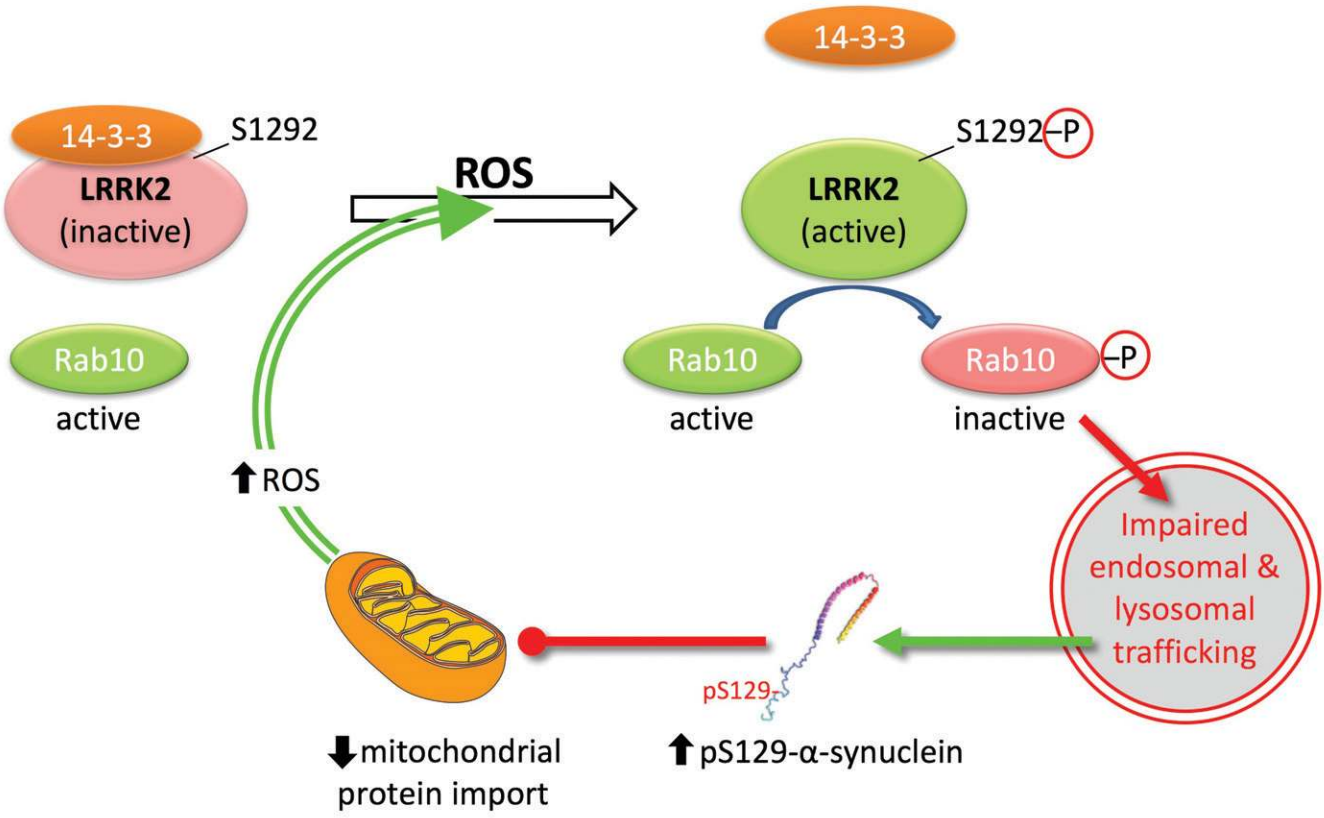
14-3-3
S1292
LRRK2
(inactive)
ROS
14-3-3
S1292–P
LRRK2
(active)
Rab10
active
Rab10
active
Rab10
–P
inactive
ROS
Impaired
endosomal &
lysosomal
trafficking
pS129
mitochondrial
protein import
pS129-α-synuclein

# Supplemental Materials

## A Central Role for LRRK2 in Idiopathic Parkinson Disease

**Summary:** *Wildtype LRRK2 is activated in dopamine neurons in idiopathic Parkinson disease and plays a pathogenic role in the disease.*

Roberto Di Maio[1,2,3], Eric K. Hoffman[1,2], Emily M. Rocha[1,2], Matthew T. Keeney[1,2], Laurie H. Sanders[1,2,4], Briana R. De Miranda[1,2], Alevtina Zharikov[1,2], Amber Van Laar[1,2], Antonia F. Stepan[5], Thomas A. Lanz[5], Julia K. Kofler[6], Edward A. Burton[1,2,7], Dario R. Alessi[8], Teresa G. Hastings[1,2], J. Timothy Greenamyre[1,2,7,†]

[†]Correspondence should be addressed to JTG (jgreena@pitt.edu).

[1]Pittsburgh Institute for Neurodegenerative Diseases, University of Pittsburgh, Pittsburgh, Pennsylvania. [2]Department of Neurology, University of Pittsburgh, Pittsburgh, Pennsylvania. [3]Ri.MED Foundation, Palermo, Italy. [4]Department of Neurology, Duke University, Durham, North Carolina. [5]Worldwide Medicinal Chemistry, Pfizer Worldwide Research and Development, Cambridge, Massachusetts. [6]Department of Pathology, University of Pittsburgh, Pittsburgh, Pennsylvania. [7]Geriatric Research, Education and Clinical Center, VA Pittsburgh Healthcare System, Pittsburgh, Pennsylvania. [8]MRC Protein Phosphorylation and Ubiquitylation Units, University of Dundee, Dundee, Scotland.

**Materials and Methods**

*Reagents*. Antibodies were sourced as follows:

| Antibody | Cat # | Company | Dilution factor |
|---|---|---|---|
| **rabbit Anti-LRRK2 (phospho S1292) (MJFR-19-7-8)** | AB203181 | Abcam | ICC – 1:1000<br>IHC – 1:500 |
| **rabbit Anti-14 – 3 - 3** | AB9063 | Abcam | ICC - 1:1000<br>IHC – 1:500 |
| **mouse Anti-Synuclein (phospho S129) [P-syn/81A]** | AB184674 | Abcam | IHC – 1:1000 |
| **rabbit Anti-LAMP1** | AB24170 | Abcam | IHC – 1:500 |
| **mouse Anti-p62/SQSTM1** | H00008878 | Abnova | IHC – 1:500 |
| **rabbit Anti-Rab10 (D36C4) Xp(R)** | 8127S | Cell Signaling | ICC – 1:1000 |
| **goat Anti-Rab10 pThr73** | S873D | Dr. Dario Alessi | ICC - 1:1000<br>IHC – 1:500 |
| **rabbit Anti-LAMP2A** | 512200 | Invitrogen | IHC – 1:500 |
| **mouse Anti-Ndufs3 (OxPhos 30 KDa)** | 459130 | Life Technologies | IHC – 1:1000 |
| **sheep Anti-TH** | AB1542 | Millipore | IHC – 1:2000 |
| **rabbit Anti-TOM 20** | sc-11415 | Santa Cruz | IHC - 1:1000 |
| **mouse Anti-LRRK2/Dardarin, clone N241A/34** | 75-253 | UC Davis/<br>NIH NeuroMab Facility<br>Antibodies incorporated | ICC – 1:1000<br>IHC – 1:500 |
| **rabbit Anti-Iba1** | 019-19741 | Wako | IHC – 1:500 |

Selective LRRK2 kinase inhibitors were obtained from the following sources: GNE-7915 (ChemieTek), MLi-2 (Dr. Dario Alessi), PF-360 (Pfizer Inc).

*Fluorescence measurements*. Quantitative fluorescence measurements were made with an Olympus upright 3-laser scanning confocal microscope, taking care to ensure that images contained no saturated pixels. For quantitative comparisons, all imaging parameters (e.g., laser power, exposure, pinhole) were held constant across specimens. Depending on the specific experiment, readouts included fluorescence intensity or number of objects (punctae) in predefined regions of interest, such as tyrosine hydroxylase-positive dopaminergic neurons or Iba1-positive microglia.

*Animals*. All experiments utilizing animals were approved by the Institutional Animal Care and Use Committee of the University of Pittsburgh. Rats were treated with rotenone as described (*36, 37*).

*AAV2-mediated gene transfer*. Details per Zharikov et al (*37*). Rats were euthanized 6 weeks after injection.

*Human tissue*. Paraffin-embedded midbrain sections were obtained from the University of Pittsburgh Brain Bank. All banked specimens have undergone standardized premortem neurological and post-mortem neuropathological assessment. Diagnoses were confirmed and staging performed by the study neuropathologist (JKK) by examination of H&E, alpha-synuclein, tau, silver and ubiquitin stains of key sections needed for Braak staging (*38*). The study design was reviewed and approved by the University of Pittsburgh Committee for Oversight of Research Involving the Dead. Midbrain sections from 7 PD/PDD patients and 8 control subjects, matched for age and postmortem intervals, were used for analysis.

| | ***Male/Female*** | ***Age*** | ***Brain weight*** | ***Postmortem Interval*** |
|---|---|---|---|---|
| ***Control*** | 5/3 | 67 ± 5 | 1248 ± 33 | 7.0 ± 0.8 |
| ***iPD*** | 6/1 | 73 ± 4 | 1297 ± 29 | 9.8 ± 1.9 |

To eliminate endogenous fluorescence, human tissue was pre-treated with an autofluorescence eliminating reagent according to the manufacturer's instructions (Chemicon, Temecula, CA).

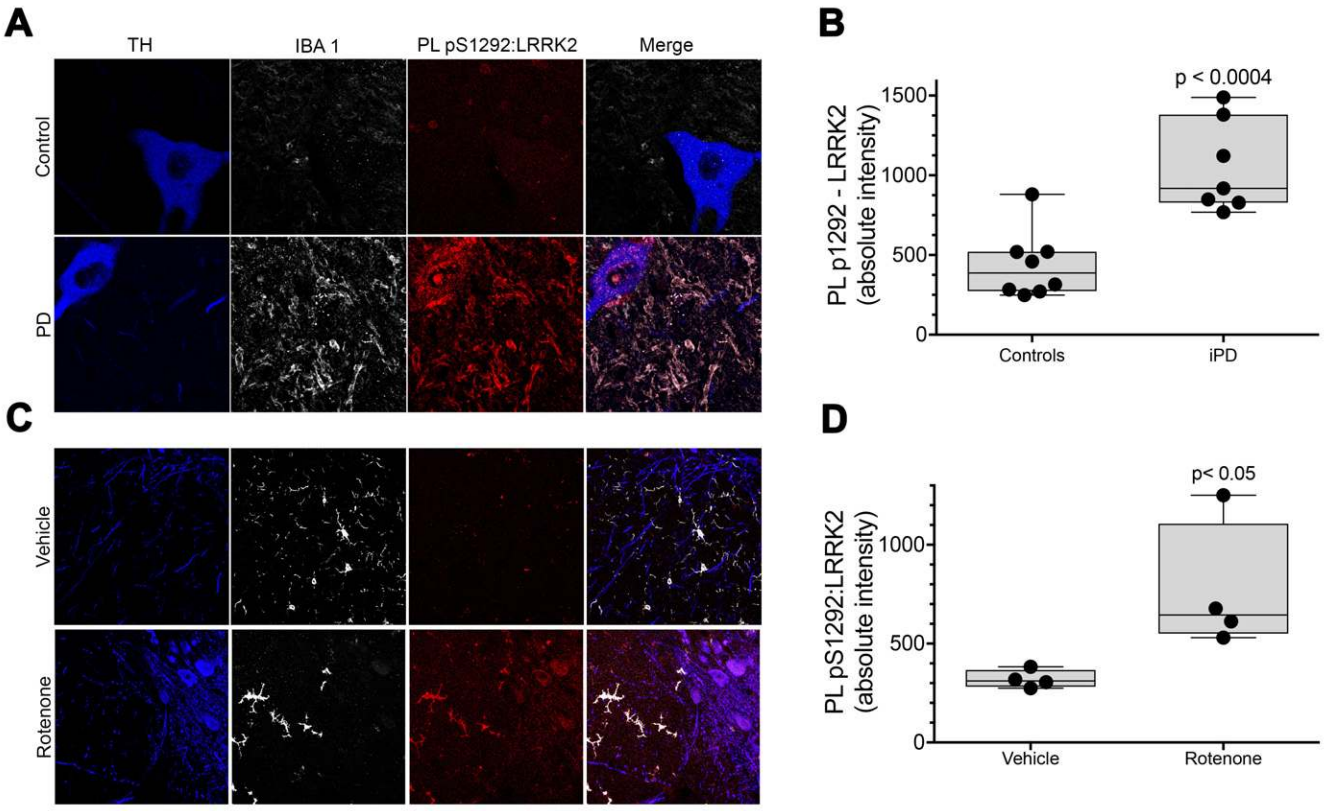


***Figure S1.*** Active LRRK2 is detected by PL in microglia in control brains and is increased in iPD and in rotenone-treated rats. **(A)** Colocalization of pSer1292 PL signal in Iba1 immunoreactive microglia in substantia nigra from control and iPD brains. **(B)** Quantification of pSer1292 PL signal in Iba1 labeled microglia in substantia nigra from 8 control and 7 iPD brains. Comparison by unpaired 2-tail t-test. **(C)** Colocalization of pSer1292 PL signal in Iba1 immunoreactive microglia in substantia nigra from control and rotenone treated rats. **(D)** Quantification of pSer1292 PL signal in Iba1 labeled microglia in substantia nigra from 4 control and 4 rotenone treated rat brains. Comparison by unpaired 2-tail t-test.

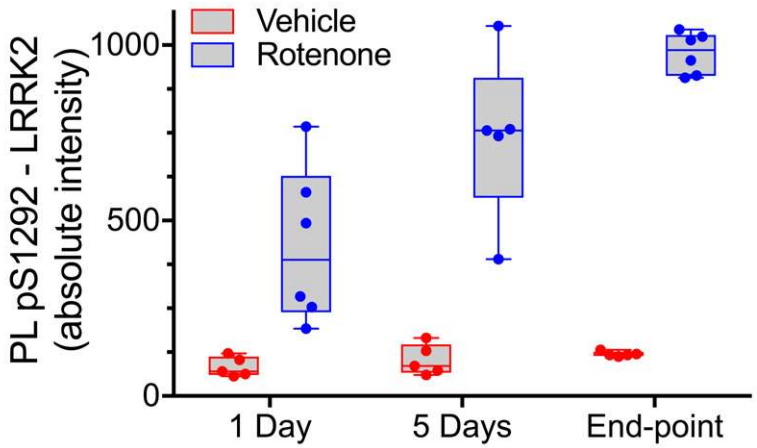


***Figure S2.*** Time course of *in vivo* rotenone-induced LRRK2 activation as assessed by pSer1292 PL signal. Note that LRRK2 is significantly activated by 1 and 5 days of rotenone treatment, time points before there is detectable neurodegeneration. "Endpoint", defined behaviorally, typically occurs at 10-14 days. The pSer1292 PL signal was significantly elevated ($p<0.0001$, ANOVA with Bonferroni correction) compared to vehicle at all time points.

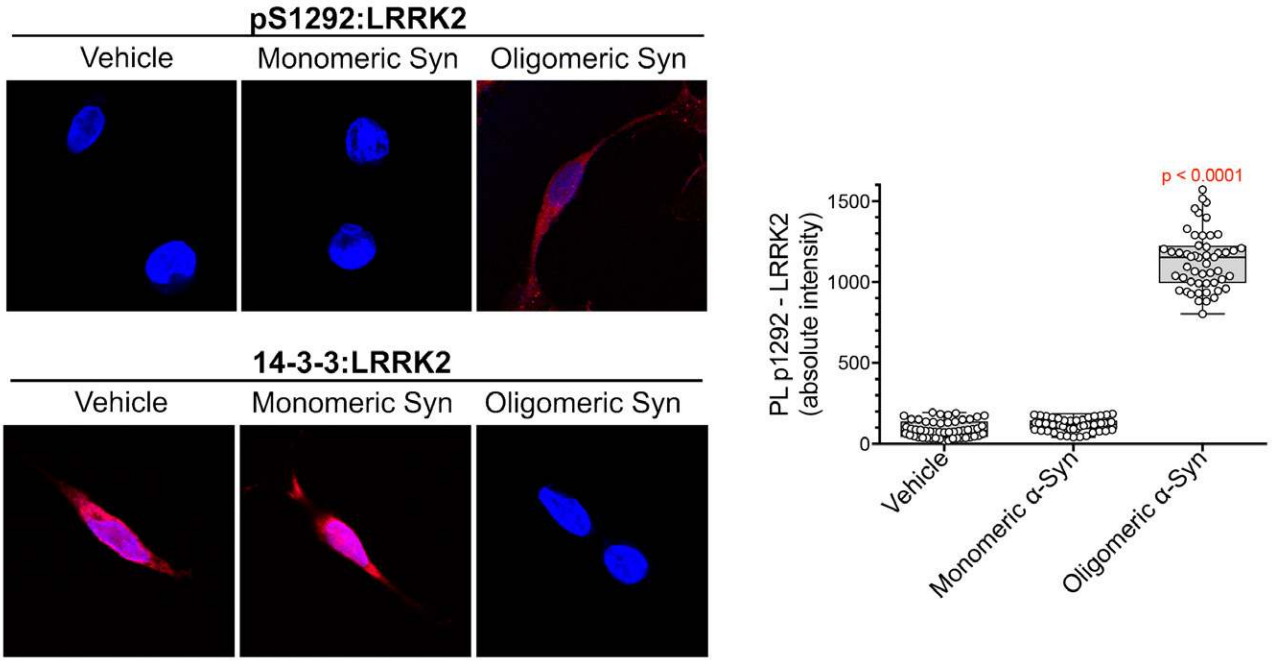


***Figure S3.*** LRRK2 is activated by oligomeric but not monomeric α-synuclein. pSer1292 PL signal (top row) and 14-3-3:LRRK2 PL (bottom row) in $SNCA^{-/-}$ cells treated with vehicle, monomeric α-synuclein or oligomeric α-synuclein. Note the increase in pSer1292 PL signal and loss of 14-3-3:LRRK2 – indicating LRRK2 activation – only in cells treated with oligomeric α-synuclein. The graph shows quantification of the pSer1292 PL signal from these experiments (N=3). Each symbol represents a single cell. Comparison by ANOVA with Bonferroni correction.

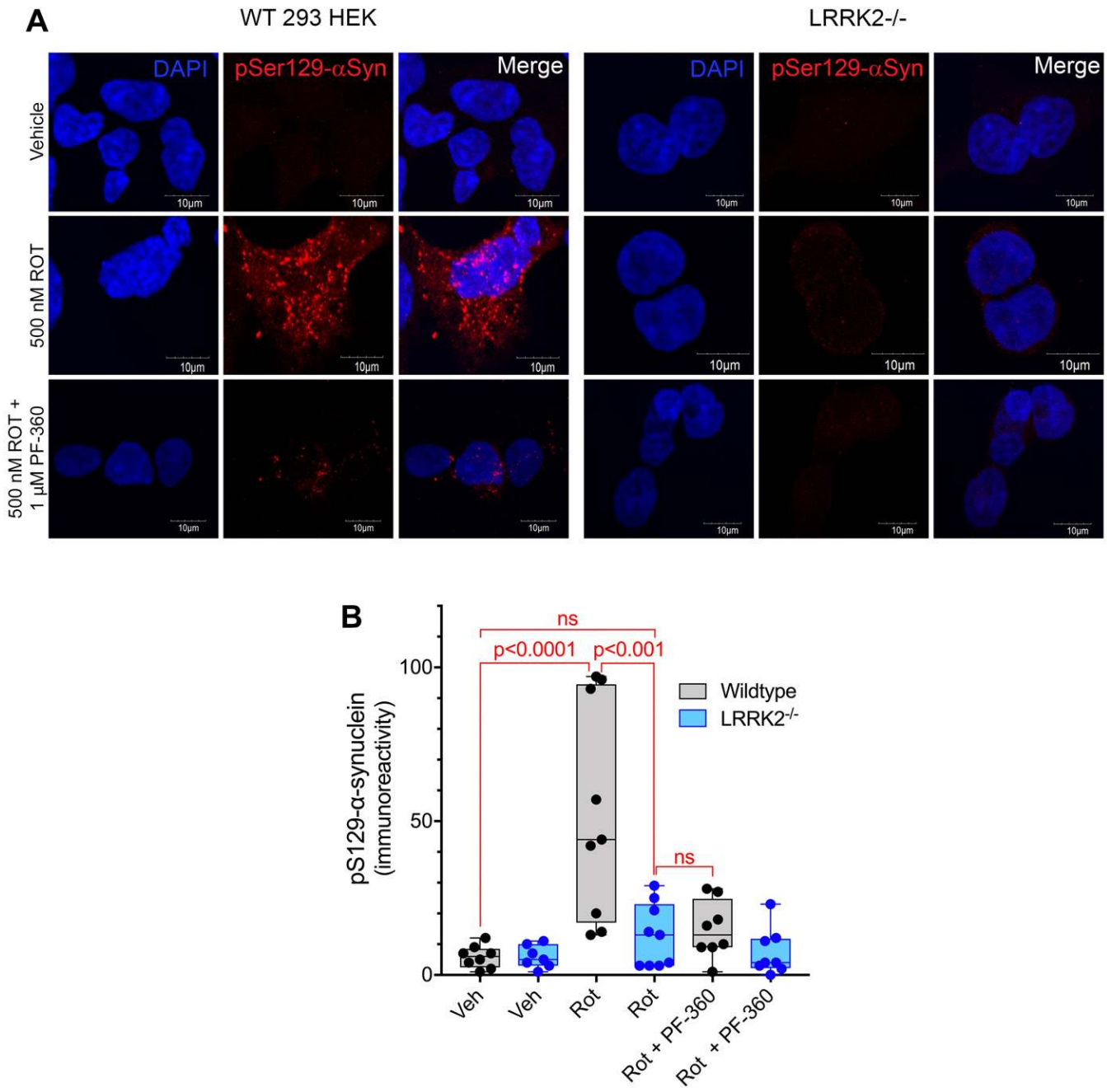


***Figure S4.*** Rotenone-induced accumulation of pSer129-α-synuclein is LRRK2-dependent. Wildtype and LRRK2$^{-/-}$ cells were treated with rotenone with or without co-treatment with 1 μM PF-360. **(A)** Representative images of pSer129-α-synuclein immunofluorescence from wildtype and LRRK2$^{-/-}$ cells. ***Red***, pSer129-α-synuclein immunofluorescence. **(B)** Quantification of pSer129-α-synuclein in wildtype and LRRK2$^{-/-}$ cells 24 hours after treatment with vehicle, rotenone, or rotenone + PF-360. Each symbol represents the mean value of an independent experiment (each with 4 technical replicates) in which immunoreactivity was measured in at least 80 cells. Analysis was by one-way ANOVA with Sidak's multiple comparisons test.